UNIVERSITY OF BIRMINGHAM

Sustainability and climate resilience metrics and trade-offs in transport infrastructure asset recovery

Mitoulis, Stergios-aristoteles; Bompa, Dan V.; Argyroudis, Sotirios

[Link to publication on Research at Birmingham portal](#)

Sustainability and climate resilience metrics and trade-offs in transport infrastructure asset recovery

Stergios-Aristoteles Mitoulis [a,1,*], Dan V. Bompa [b], Sotirios Argyroudis [c,1]

[a] *Department of Civil Engineering, School of Engineering, CEPS, University of Birmingham, UK*
[b] *School of Sustainability, Civil and Environmental Engineering, University of Surrey, UK*
[c] *Department of Civil and Environmental Engineering, CEDPS, Brunel University London, UK*

A B S T R A C T

Climate change exacerbates natural hazards and continuously challenges the performance of critical infrastructure. Thus, climate resilience and sustainable adaptation of infrastructure are of paramount importance. This paper puts forward a novel framework and metrics for optimising *sustainability* (Greenhouse Gas emissions - GHG), *climate resilience* (restoration time), and *cost*. The framework aims to facilitate decision-making by operators and stakeholders and communicate actionable trade-offs between these principles. It describes approaches for quantifying ex-ante adaptation and ex-post recovery from the lenses of sustainability and resilience using relevant metrics. This paper concludes with an application of the framework on a bridge, where normalised metrics are integrated into one unique index (I_{SRC}), which can be used in the recovery prioritisation for portfolios of similar assets. The optimisation program includes a bridge recovery, while reducing GHG emissions. The impact of climate change on the sustainability and resilience indexes is examined and the results show how the optimum solutions are adversely affected by different climate projections. In all scenarios examined, more sustainable solutions leading to reduced GHG emissions (tCO2e) are the optimum solutions when weighing resilience and cost. Based on the case study analysed in this paper, the low carbon restoration strategy resulted in up to 50% higher I_{SRC}, which can justify investments for low GHG adaptation strategies in transport assets.

1. Introduction

Engineers, decision-makers, and transport infrastructure operators are striving to design, construct, and maintain infrastructure, which is resilient and sustainable. Nevertheless, available design guidelines do not directly support these principles. There have been disparate frameworks and tools used for combining these two concepts, which in some cases are synergistic and in others conflicting. Some frame sustainability and resilience as synergistic principles, while others describe them as different and/or competing design targets (Marchese et al., 2018). As a result, it is challenging to optimise the performance of large-scale transport infrastructure systems and assets (Shani et al., 2021) based on these principles, even though this seems to have been systematically done for buildings (Sharif and Hammad, 2019). Optimising the resilience of transport assets, such as bridges, to climate hazards, considering environmental

impacts due to e.g. whole life carbon emissions, and cost, is a first vital step toward combining the two principles into an integrated framework and global metrics.

Transport assets are exposed to natural hazards, often exacerbated by climate change, such as floods and extreme temperatures, as well as inherent deteriorating mechanisms e.g., ageing and other human-induced hazards (Mitoulis et al., 2023) leading to failures and road closures throughout their lifespans. These disruptions have severe impacts on world economies, peoples' safety, and perturbations to the supply chain (Haraguchi and Lall, 2015). In addition to the economic importance of transport infrastructure, their construction and operation totals more than 70% of the world-wide Greenhouse Gas (GHG) emissions (Saha, 2018). Various GHG are represented through a carbon (CO_2) equivalence to quantify environmental impacts (Horvath, 2005).

In the US, 36% of bridges need repair work (ARTBA 2021[2]) and their cost is estimated at $125 billion based on the ASCE Report Card History (2021). Approximately 53% of the bridge failures are caused by hydraulic actions, such as floods and scour (Wardhana and Hadipriono, 2003), a number that is likely to be higher these days due to climate exacerbations. These values are generally mirrored worldwide as a function of the country's GDP, making infrastructure sustainable development a key concern to achieving 2030 emission targets and net-zero by 2050 (European Commission, 2019; Mitoulis et al., 2021a). A recent example of the extensive destruction of bridges and transport networks due to a flash flood was the 2020 Medicane Ianos that struck Greece and affected a large part of the country. Five bridges were severely damaged and/or collapsed, while a further three bridges were extensively damaged (Loli et al., 2022). These failures had a profound impact on the transport services, due to the low redundancies of the sparse road network of the region, while resulted in long detours, additional CO_2 and noise emissions, in an environmentally sensitive area. This event highlighted the significance of transport networks to be resilient and for recovery strategies to incorporate sustainable measures with minimal environmental impact.

In this background context, the motivation for this research paper is to optimise the recovery strategy in transport infrastructure assets with focus on bridges, from the lenses of sustainability and resilience, using representative metrics, i.e., GHG emissions, cost, and duration of reconstruction. This application included an optimisation that considered the recovery time of a bridge in the aftermath of a flood, which is a measurable property of resilience, while the quantification of sustainability is performed on the basis of upfront carbon emission estimations, as a result of the restoration tasks. Thus, the contributions of this work include a framework for consolidating sustainability and climate resilience in the post-disaster recovery of transport assets, and a method for transport operators to facilitate decision-making using global metrics that integrate sustainability and resilience. Though the research is focusing on bridges, the framework can be used as a roadmap for optimising sustainability and resilience in other critical assets.

2. Literature review

This section provides a critical review of the available climate resilience frameworks for transport infrastructure, and the frameworks, standards, and databases for assessing carbon emissions, based on which the direct impacts on sustainability are evaluated. Emphasis is put on the optimisation of repair and recovery, relative to CO_2 life cycle impacts. The section concludes with gaps in the knowledge, which prevent us from delivering optimised climate resilience and low-carbon emission solutions in transport infrastructure.

Resilience is the ability of infrastructure, operations and dependent communities to withstand and recover swiftly from low frequency high-impact events that change its capacity, operability and function. In civil infrastructure systems, such as transport networks assets, e.g. bridges, resilience is commonly measured with the ability to gain a target operability level, e.g. traffic, after the occurrence of an extreme event, such as a flash flood, and to reinstate its functionality swiftly. In this paper, the resilience is quantified for a transport asset based on the four dimensions, also known as the 4R of resilience, described by Bruneau et al. (2003). Since this paper deals with a transport asset, emphasis is placed on the dimension, properties and results for this asset. The framework for the quantification of the resilience of systems of assets was described in detail in Argyroudis et al. (2020). In bridges, **Redundancy** is a structural property that mainly refers to its structural system and ability to redistribute loads in case of damage. It is increased when alternative paths and load transfer mechanisms are available, for example, integral bridges with monolithic connections are structurally more robust in comparison with their isolated counterparts (Mitoulis, 2020). **Robustness** is described as the ability of the bridge to resist the impact of hazard events, e.g. flash flood of a given intensity. Robustness and redundancy are typically quantified by fragility, vulnerability, and functionality loss functions (Argyroudis et al., 2019; McKenna et al., 2021). **Rapidity** is a property that describes how quickly the bridge or other transport assets recover after an event. This depends on the damage state, the availability of resources (**Resourcefulness**) and the targeted operability. Rapidity is expressed by restoration and reinstatement models, which correlate the recovery time with the gain in structural capacity and operability (e.g., traffic), respectively. In that case, downtime is also critical for the estimation of indirect losses, which are related to the duration of the restoration of the affected components (Smith et al., 2021; Alipour and Shafei, 2016). Accelerated bridge constructions have been proposed for bridges in earthquake-prone areas (Piras et al., 2022; Marriott et al., 2009), to increase their resilience, yet these structural schemes have not been employed for other hazards.

Sustainability is central to governments, non-governmental organisations, communities, and private stakeholders. It is embedded in all levels of infrastructure development and management, including the construction of new and existing infrastructure assets and networks. For the repair of existing assets, the main aims are to minimise the environmental damage produced of the construction

---
[2] https://artbabridgereport.org/reports/2021-ARTBA-Bridge-Report.pdf.

materials, processes, and activities. Life-cycle assessments (LCAs) are carried out to quantify the environmental impacts by a process, product, or system by estimating the energy, materials, and waste produced, as well as to minimise burdens (ISO, 2006). These impacts are typically based on region-specific life-cycle inventories, and require a system boundary and a functional unit, as defined below.

Khanna et al. (2022) and Ecochain Mobius platform describe the 15 categories of environmental impacts in LCA. The system boundary gives the limits to which the LCA is assessed (e.g., module A1-A3 'cradle to the factory gate', or modules A-D 'cradle-to-cradle' described below), whilst the functional unit is used to measure the performance of products, processes or activities. The latter is adopted to compare different alternatives having identical utility for the same function (Santos et al., 2018). Typical functional units in construction materials are cubic metres [m^3] for concrete, kilograms [kg] for steel, square metres [m^2] for pavements or metres [m] for motorways. In construction, the environmental damage is generally expressed through the Global Warming Potential (GWP), which is used to quantify the impact of climate change. GWP considers the effects of various Greenhouse Gases (GHG) through a carbon equivalence (Horvath, 2005).

The whole-life carbon is divided into embodied and operational components. The former (modules A1 to A3) refers to the quantity of carbon associated with the extraction, refinement, processes and transportation of materials (CEN, 2022). Modules A4 and A5 refer to the construction stage carbon, which is associated with fabrication, assembly, and transportation to the site, as well as other carbon due to waste, temporary works and other onsite activities. Operational carbon is due to emissions occurring during the asset operation (stage B). The whole-life carbon also includes end-of-life carbon associated with decommissioning (stage C), as well as include stage D in which benefits and loads beyond the asset life-cycle, such as recovery or recycling, are considered.

Process or product-based LCAs were used extensively for evaluating emissions of construction materials, processes and activities (Achilleos et al., 2011; Maxineasa et al., 2017; Sabău et al, 2021). Life-cycle appraisals were carried out on road construction projects worldwide to provide quantitative results for informed decision-making for asset management (Reza et al., 2014; Wang et al., 2015; Somboonpisan and Limsawasd, 2021; Nahangi et al., 2021).

Dong et al. (2013, 2014) assessed the temporal variability of carbon emissions of bridges and infrastructure networks to multiple hazards, taking into account the structural deterioration. Carbon emissions were used elsewhere as a performance metric in estimating the resilience for several seismic intensities and bridge typologies considering a range of seismic intensities, in combination with repair cost and repair time (Mackie et al., 2016). Independent of conventional LCA frameworks (e.g., CEN 2022), the study considered three main life-cycle phases specific to the repair of an infrastructure asset depending on damage states: on-site emissions, emissions outside of the site, emissions due to the production of materials.

On-site emissions are largely generated by the construction equipment operation, which can account for between 10 and 20% of the total emissions of a project, using conventional equipment (Noland and Hanson, 2015). The magnitude of these emissions largely depends on the site conditions and can vary by a factor of 30 when flat sites and mountainous areas are considered (Barandica et al., 2013). Using hybrid engines or more sustainable alternatives can reduce equipment emissions by up to 50% (Somboonpisan and Limsawasd, 2021). Transportation typically contributes to around 4% or less for typical haulage needs (Mackie et al., 2016), and reductions can be obtained by similar measures.

Up to 80% of the emissions are typically generated by material production, whilst only 3% and 10% of the total emissions come from material transportation and onsite activities (Wang et al., 2015). In bridge projects, 98% of carbon emissions are from steel and cement, which only account for around 15% of the total quantity of materials employed, whilst rock and sand count less than 1% of the total amount of carbon and are 80% of the amount of the total material (Liu et al., 2019). Low-carbon and high-performance materials can however provide over 40% carbon reductions in bridge projects compared with conventional alternatives (Keoleian et al., 2005). Road surfacing can count between 2 and 37% of total emissions, depending on the type of pavement with cement pavement having 12% and 55% less environmental effects and energy consumption than asphalt pavements (Heidari et al., 2020). Though not directly related to the emissions associated with the post-hazard recovery, the pavement flexibility and reduction of rolling resistance can underestimate extremely important impacts over the asset lifetime (Santero and Horvath, 2009).

Infrastructure networks have relatively long lifetimes, are subjected to a number of interventions during operation and are unlikely to be completely decommissioned (Saxe and Kasraian, 2020). LCAs on transport networks indicated a lack of standardised approaches for functional units, system limits, network impacts, and the possibility of burden offsetting (Jiang and Wu, 2019), including direct and environmental costs (Wang et al., 2020). This is particularly because existing LCA methods are product-based and do not reflect the life-cycle specificity of infrastructure networks. For recovery interventions in post-hazard situations, such as floods and earthquakes, product-based LCAs can be adopted as long as the temporal scale is limited to the commissioning of the restored asset.

Despite the developments in the areas of sustainability and resilience **optimisation** (Santos et al., 2022; Peng et al., 2022; Frangopol et al., 2017) and the numerous frameworks published for quantifying them (Wan et al., 2018; Qian et al., 2022), there has been very little research on the trade-offs between these two fundamental principles in a quantifiable manner in transportation infrastructure. This is mainly because it is unknown when these two principles are synergistic or competing with each other (Marchese et al., 2018). There have been very few papers that delivered a unified approach to sustainability and resilience (Bocchini et al., 2014) from an economic losses point of view (Lounis and McAllister, 2016) and from a resilience-sustainability correlation metrics point of view, at the asset (bridge) and network level (Vishnu et al., 2022; Tan et al., 2022). However, none of these research endeavours dealt with sustainability climate resilience for transport assets and this is an acknowledged gap.

3. Framework for optimising sustainability and climate resilience

This paper delivers a framework for optimising sustainability and climate resilience, based on tCO$_2$e i.e tonnes (t) of carbon dioxide (CO2) equivalent (e) and proposes a global metric (I_{SRC}). The paper uses a benchmark transport asset i.e. a typical river-crossing 3-span
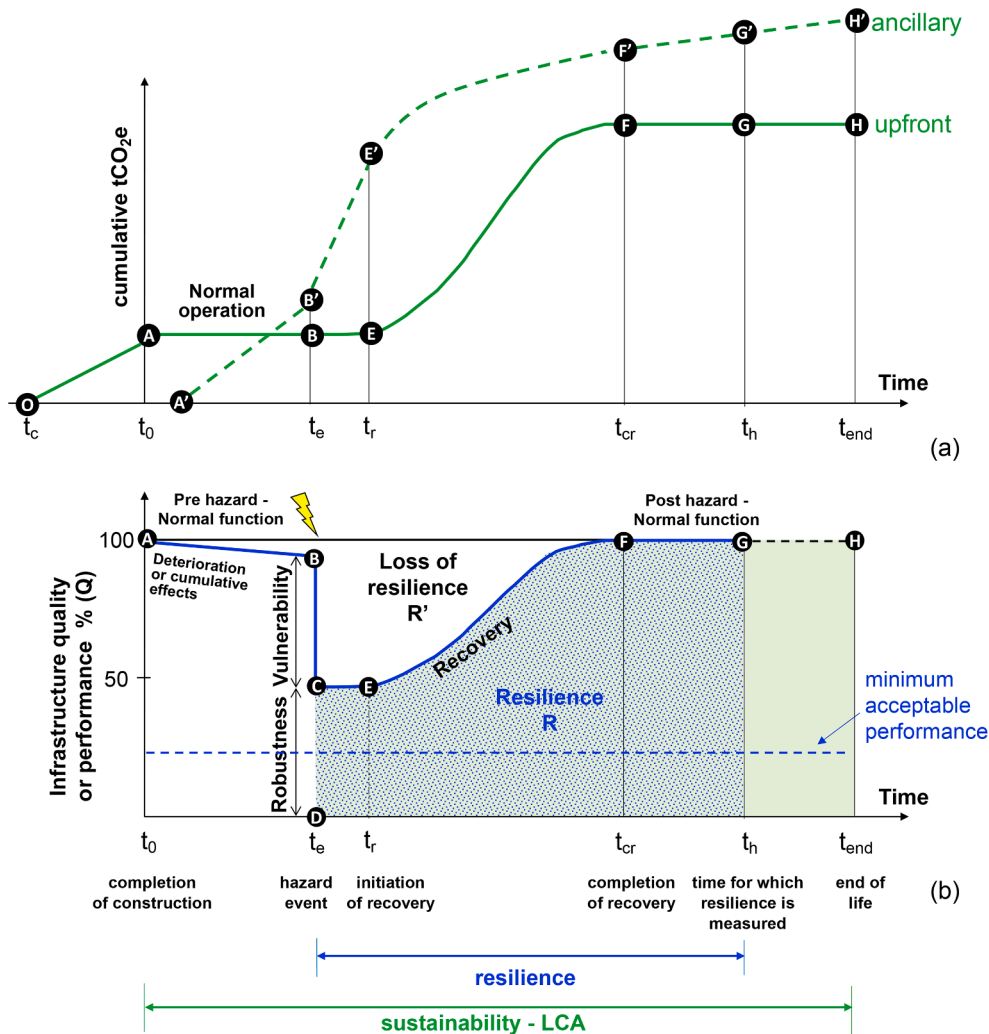
O: commencement of construction,
A: completion of construction, bridge open to traffic
AB: bridge operates with minimal maintenance or inspection
A'B': tCO2e increase because the bridge operates with decreased functionality and as a result
       vehicle detours are required
BE: bridge is damaged, but no action is taken (idle time)
B'E': tCO2e increased rapidly as bridge is partially/completely closed and as a result traffic is diverted
EF: restoration measures are being implemented
E'F': ancillary tCO2e due to the implementation of restoration measures, including traffic detour
FH: post-disaster normal function, no maintenance
F'H': similar to A'B'

Fig. 1. Baseline scenario, without regular maintenance. (a) Evolution of cumulative tCO_2e. Solid line shows upfront and dashed line shows ancillary tCO_2e and; (b) resilience, expressed as quality or performance of transport infrastructure responding to a hazard occurrence.

bridge described by Argyroudis and Mitoulis (2021) and Mitoulis et al. (2021), for which sustainability and resilience are optimised, by analysing and quantifying alternative restoration strategies for nine flood scenarios, leading to different extents of foundation scour and different global metric (I_{SRC}) values. The paper concludes with different climate projections and demonstrates the impact of exacerbations of hazard occurrences on resilience, sustainability, cost and on the global metric I_{SRC}.

Before the description of the framework, sustainability and resilience are described schematically, based on cumulative tCO_2e as a metric of sustainability, and infrastructure performance as a measure of resilience. The conceptual plots of Fig. 1, Fig. 2, and Fig. 3 are referring to the case of a critical transport asset that has been impacted by a major stressor (e.g., flood), and appropriate measures are taken to reinstate its capacity (strength) and functionality (e.g. traffic). The three figures show three cases. Fig. 1 is the benchmark,

O: commencement of construction,

A: completion of construction, bridge open to traffic

AB, CD, EF, GH: bridge operates with standard maintenance

BC, FG: proactive adaptation measures

DE: recovery after hazard event (see Fig. 1, B to F)

HJ: bridge is not maintained-end of life

A'B', C'D', E'F', G'H', H'J': tCO2e increase due to ancillary maintenance measures, but less vehicle detours compared to Fig. 1.

B'C', D'E', F'G': tCO2e increased rapidly as bridge is partially/completely closed and as a result traffic is diverted, maintenance/restoration measures are being implemented
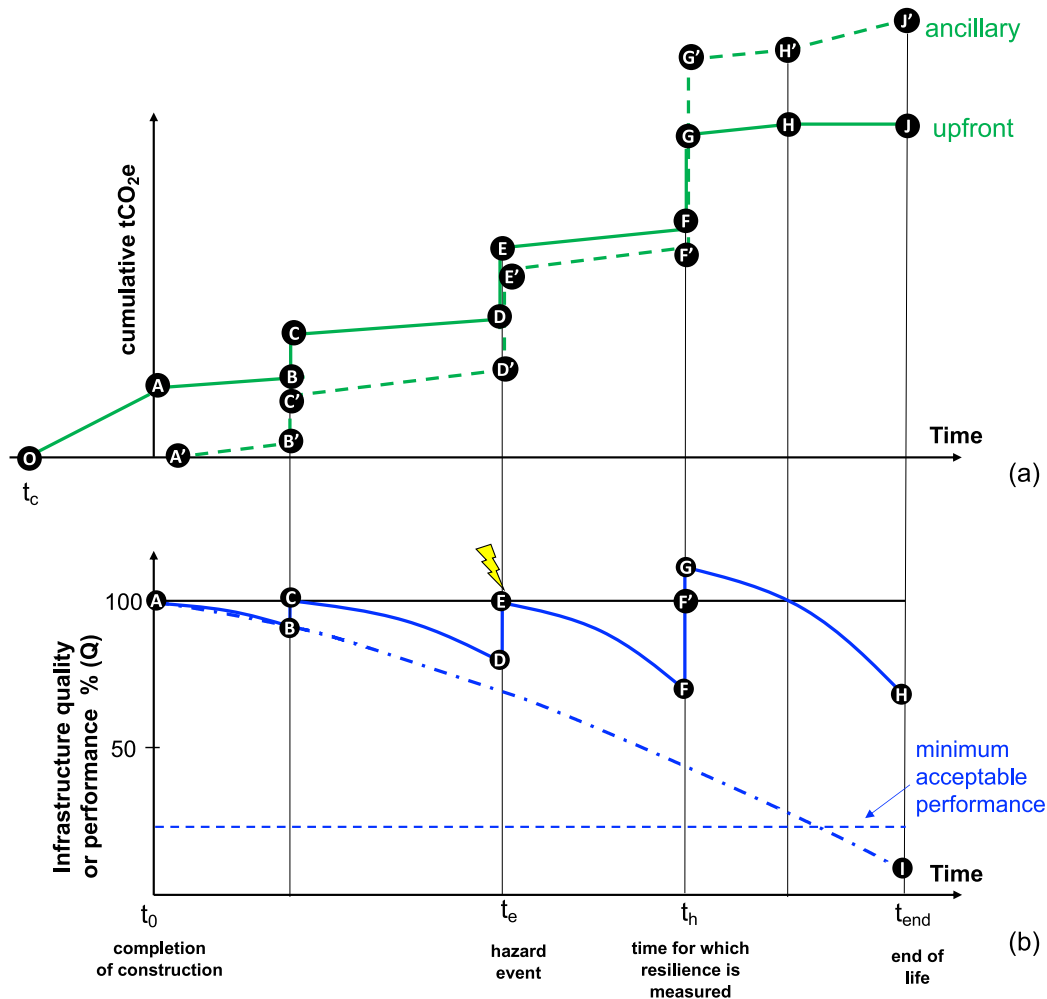
AI: deterioration of infrastructure quality throughout its life

BC: proactive adaptation measures and/or maintenance

DE: restoration after a climate hazard occurrence (see Fig. 1, C to F)

FG: enhancement of infrastructure performance with adaptation measures

GH: operation until the end of life

Fig. 2. With proactive (ex-ante) adaptation and/or regular maintenance. (a) Evolution of cumulative tCO$_2$e. Solid line shows upfront and dashed line shows ancillary tCO2e and (b) resilience, expressed as quality or performance of transport infrastructure including adaptation and response to hazard occurrences. Dot-dashed line illustrates the hypothetical case where the asset reaches the end of its lifespan without any maintenance or hazard occurrences.

O: commencement of construction,
A: completion of construction, bridge open to traffic
AD: bridge operates with standard maintenance
DG, DF, DE: tCO2e due to reactive measures (partial, fully restoration and beyond the original capacity)
A'D': tCO2e increase due to maintenance measures, more detours in comparison to Fig. 2
D'G', D'F', D'E': tCO2e increased rapidly as bridge is partially/completely closed and as a result traffic is diverted, reactive measures are being implemented
Note: reactive measures result to higher tCO2e
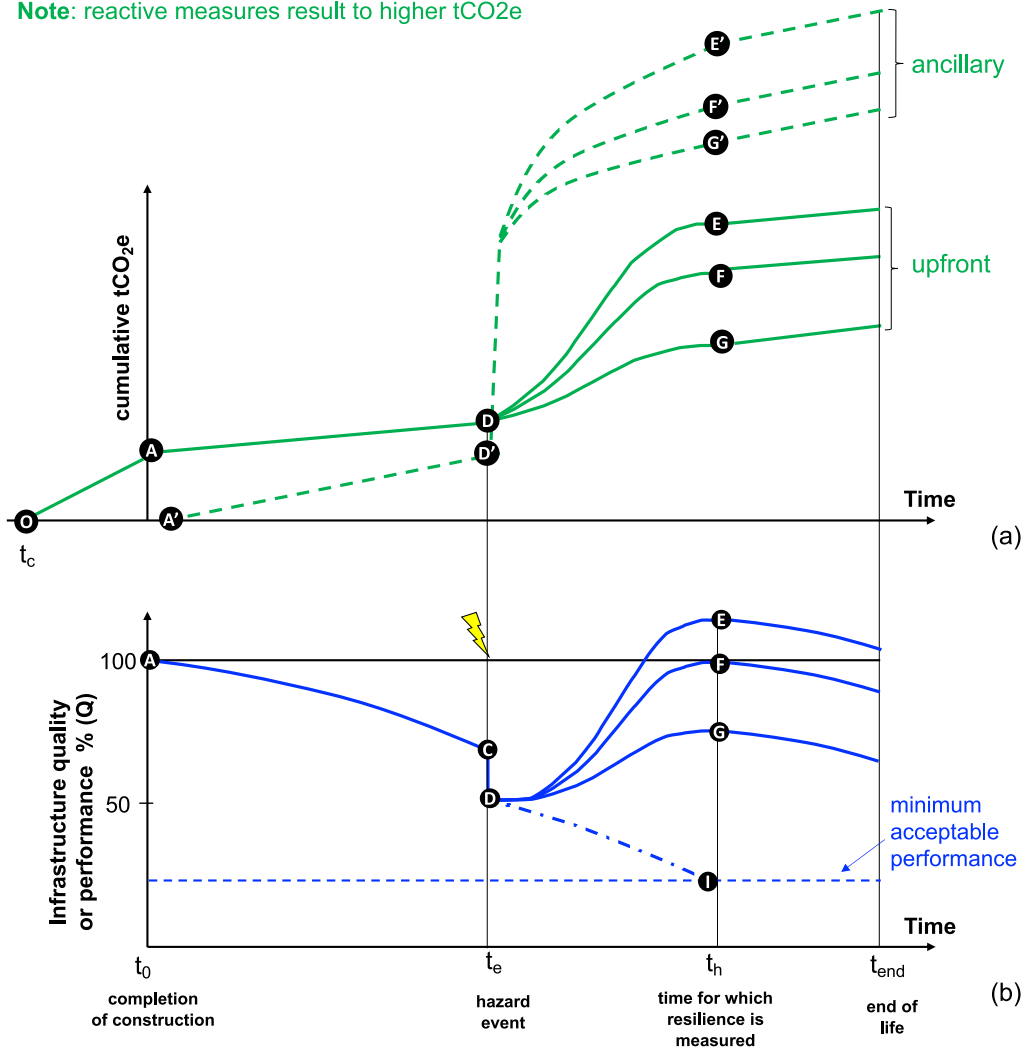
AI: deterioration of infrastructure quality throughout its life
CD: loss of performance due to hazard occurrence
DG: reactive measures, partially restored
DF: reactive measures, fully restored
DE: reactive and adaptation measures beyond the original capacity

Fig. 3. With reactive (ex-post) recovery measures. (a) Evolution of cumulative tCO_2e. Solid line shows upfront and dashed line shows ancillary tCO_2e for three different scenarios (i.e., smaller, equal, higher than the original performance) and; (b) resilience, expressed as quality or performance of transport infrastructure including adaptation and response to hazard occurrences.

Fig. 2 illustrates the case where the asset is maintained throughout its life and hence ex-ante adaptation measures and maintenance take place, whereas Fig. 2 and Fig. 3 represent the case of ex-ante and ex-post restoration of well-maintained and poorly maintained assets correspondingly. Fig. 1a, Fig. 2a, Fig. 3a illustrate the upfront (solid lines) and ancillary tCO_2e (dashed lines), due to the

construction (see paths OA), and maintenance of the asset throughout its life. In all cases, the ancillary tCO2e are shown to be higher than the upfront, due to the detour of the traffic during maintenance and restoration. Also, Fig. 3a, shows greater ancillary and upfront tCO2e than Fig. 2a, to highlight the importance of preventive maintenance, which leads to more sustainable solutions in comparison with emergency recovery in the aftermath of natural hazards. Fig. 1b, Fig. 2b, Fig. 3b illustrate the resilience curves of the same transport asset throughout its lifetime. The area under the resilience curve is a metric of resilience (R index) (Argyroudis, 2021). Again Fig. 2b that shows ex-ante adaptation and preventive maintenance leads to higher resilience in comparison with Fig. 3b, which corresponds to an unmaintained asset and will respond poorly during hazard occurrences leading to a longer recovery time. It is noted that in transport assets, the resilience is typically measured for the time window between the hazard event occurrence (t_e) and time t_h, which could be the time when the recovery is completed. Instead, sustainability refers to the entire lifespan of the asset (see e.g., LCA as shown in Fig. 1). All figures include a detailed description of the characteristic points and paths.

Fig. 1 provides an illustration of the infrastructure quality or performance as a metric of resilience and the emission of tCO2e, as a metric of sustainability. In Fig. 1a, the upfront tCO2e, typically owed to the use of materials, and the application of restoration tasks is shown with the solid line. Ancillary tCO2e emissions, due to e.g., traffic detours, are illustrated with the dashed line. Initially, the resilience has a small drop due to e.g., deterioration effects, which could be due to the corrosion of tendons and traffic increase. The gradual loss of bridge functionality may lead to occasional detours, and hence tCO2e, which are shown with the line A'B' in Fig. 1a. The figure refers to the case where no frequent maintenance takes place and as a result, the occurrence of a hazard event is likely to lead to a significant loss of performance of the asset, e.g., the bridge and as a result, a rapid increase is tCO2e between B'E' and a smaller rate of tCO2e after the restoration of the bridge commences (see point E on the resilience curve of Fig. 1b). After the completion of the recovery, the asset functions with its normal operability which leads to no additional direct tCO2e, and a small increase in indirect tCO2e (see F'H'), similarly to the A'B'.

Fig. 2 and Fig. 3 illustrate tCO2e and performance over time for ex-ante and ex-post adaptation and recovery. Fig. 2 shows frequent corrective maintenance measures (see e.g. BC, DE, FG) and as a result, the resilience of the asset is expected to be higher in comparison to Fig. 1 and Fig. 3. Similarly, the carbon emissions (Fig. 2a), are expected to be lower than the those shown in Fig. 1 and Fig. 3. The latter (Fig. 3) shows an unmaintained transport asset which is unprepared for an extreme hazard occurrence, e.g., a flood. As a consequence, the asset suffers a drastic reduction in its performance shown by the drop (CD) of the resilience curve. For a severely deteriorated (AC) and damaged asset (CD) like this, the operator will have to make a decision if the asset will be restored to its original functionality (DF) or a lower performance would be acceptable (DG) given the condition of the asset. Path DE shows the rare case where the asset is upgraded to a performance level higher than the original one. Regarding the impact on sustainability, this solution is expected to be the worst as both upfront and ancillary tCO2e are expected to be higher. This is because the use of materials, which have the largest impact on carbon emissions, is expected to be increased, while unforeseen traffic disruptions and reduced accessibility are expected to increase the ancillary emissions.

The new framework based on which resilience of critical transport infrastructure and sustainability measured on the basis of carbon emissions are optimised is shown in Fig. 4. The flowchart includes eight steps toward decision-making and indicates interdependencies, input and output between the steps. These steps are described below.

Step 1. In this step, the hazard intensity measures (IM) are defined based on predicted, measured or estimated hazard data, using e. g., high-resolution flood maps to deduce probabilistic relationships of established IM, e.g. peak water depth, streamflow velocity, and discharge, for each one of the affected assets. Depending on the stressor based on which the fragility model is built in step 2, such as scour or hydraulic forces, analytical solutions from the literature can be used (Pizarro et al., 2020) to estimate the IM for a given hazard intensity. The fluctuations in the IM, e.g., peak river flow, can be linked to the increased annual probability of exceedance, i.e., the frequency of the hazard, as a result of climate change projections (Sayers et al., 2020). Based on these projections, information on the potential range of climate exacerbations of floods in the specific location, for different return periods, and emission scenarios can be defined (Kay et al., 2021). The probability of exceedance, P_R, in T_L years of the hazard action, e.g., 50 to 120 years for highway and/or railway bridges (Thompson and Ford, 2012), is a function of the mean return period, T_R, of this level of the hazard action as per Eq. (1) (CEN, 2005).

$$T_R = -\frac{T_L}{\ln(1-P_R)} \tag{1}$$

Step 2. The vulnerability for the as built and the deteriorated asset is estimated using fragility functions from the literature. The curves correlate the probability of exceeding given damage states (e.g. minor, moderate, extensive, complete) with the hazard IM. Regarding the generation of fragility curves for transport assets this can be found in e.g., Argyroudis et al. (2019), Argyroudis and Mitoulis (2021), McKeena et al. (2021). The fragility is linked to the remaining functionality after the hazard occurrence for the different damage levels, also described in step 3 below (Karamlou and Bocchini, 2017). The fragility curves are typically defined by a lognormal probability distribution, as per Eq. (2).

$$P_f(DS \geq DS_i|IM) = \Phi[\frac{1}{\beta_{tot}}\ln(\frac{IM}{IM_{m,i}})] \tag{2}$$

where $P_f(DS \geq DS_i|IM)$ is the probability of exceeding a damage state DS, for a given intensity measure, IM, e.g. peak flow for river flood, Φ is the standard cumulative probability function, $IM_{m,i}$ is the median IM, that leads to the exceedance of i_{th} DS, and β_{tot} is the total lognormal standard deviation.

Step 3. The asset recovery is evaluated based on restoration (structural capacity) and reinstatement (traffic capacity) models,
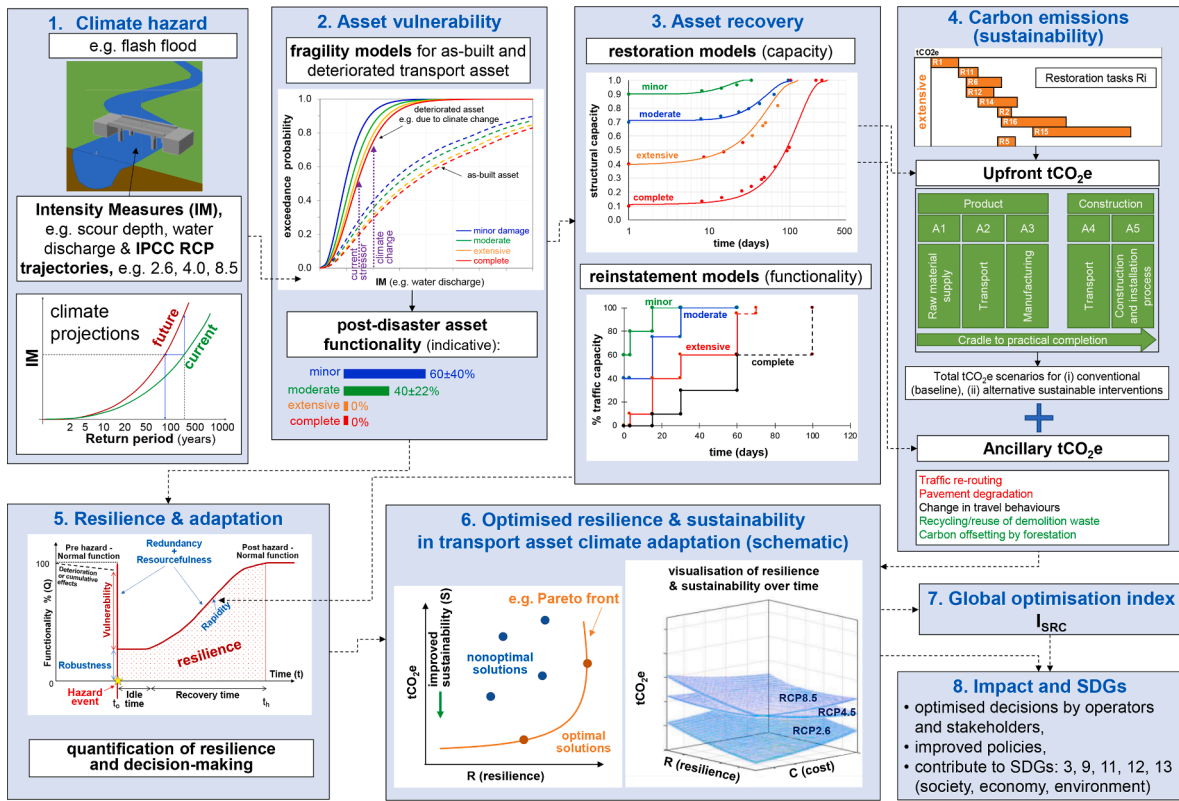
Fig. 4. Framework for sustainability (carbon emissions) and resilience optimisation for transport infrastructure climate adaptation.

which correlate the asset functionality to the recovery time after the event, considering its typology, damage state, available resources, and post-hazard idle times. In this paper, the modelling of the recovery strategies followed available models from the literature (Mitoulis et al., (2021).

Step 4. In this step, the whole life carbon emissions are quantified. The impact assessments were undertaken by employing the Intergovernmental Panel on Climate Change (IPCC, 2021) approach. To estimate the environmental impacts associated with materials, systems and works within a system boundary, the global warming potential (GWP) measured in tCO2e or kgCO2e was considered, primarily since is the main metric adopted by the construction industry worldwide. For brevity, this is referred to as carbon in this paper. The GWP is the sum of warming potential due to fossil, biogenic and land use and land use change (IPCC, 2021). However, for construction works the biogenic emissions are insignificant, and the emissions associated with land use are generally less than 5 % of GWP total and can be disregarded (CEN, 2021).

The system boundaries of the life-cycle assessment (LCA) considered herein are depicted in Fig. 5. The system is divided into two main emission groups: (i) the *upfront* emissions, correspond with the carbon associated with the construction works included in the restoration tasks at the stages shown below; (ii) whilst the *ancillary* emissions refer to the environmental impacts related to traffic re-routing, pavement degradation, change in travel behaviours or recycling and reuse of materials from construction and demolition works within a restoration task. The data flows are assessed per restoration work and use established functional units for materials and processes, e.g., 1.0 m^3 for concrete or 1.0 kg for steel. These are subsequently converted into carbon emissions, based on the estimated bills of quantities and corresponding carbon equivalent factors listed in Table A1. In this paper, the bill of quantities including the materials, on-site activities and transportation are based on the established methods typically used for bidding (Popescu et al., 2007; Spain, 2014). The assumptions considered for estimating the quantities and equipment use for each restoration task are given in Table A2. The construction equipment fuel consumption rate is based on manufacturer datasheets adopted commonly in infrastructure projects (Michaels, 2007).

The emissions can be assessed with Eq. (3), in which λ_f is a scalar factor to account for the restoration task duration described in Section 4 ($\lambda_f = 1$ for mean durations), Q is the quantity of the pollutant emitted to the environment and F is the equivalent carbon factor. The subscript i indicates the material or process, whilst subscript m is for the life-cycle phase (materials, onsite activities or transport).

$$tCO2e_j = \sum \lambda_f Q_{i,m} F_{i,m}$$

(3)

The system boundaries adopted here correspond to a '*cradle-to-practical completion*' approach, which include the product stage (modules A1-A3) and construction process stage (modules A4-A5). In terms of the construction sequence, this refers to activities
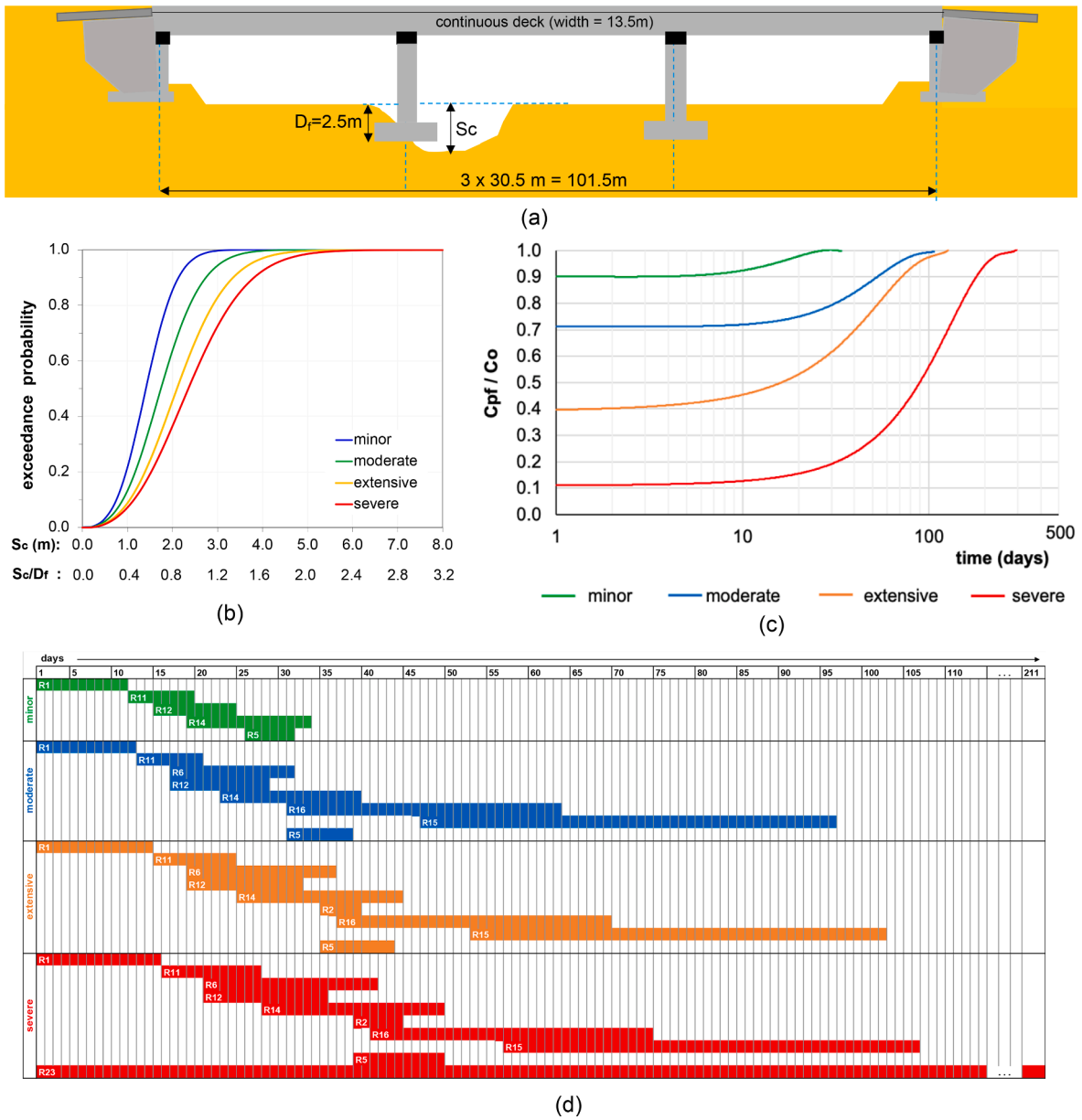
Fig. 5. (a) The reference bridge of the case study. (b) Fragility curves of the bridge as a function of the scour depth (Sc) and the normalised Sc / D_f (D_f: foundation depth). (c) Restoration curves of the bridge as a function of time (C_{pf}: post-flood capacity, C_o: original capacity), and (d) Sequence of restoration tasks for the four damage states (minor, moderate, extensive and complete). Description of the activities per task is given in Table A2.

covered from the post-planning stage to the handover. For example, concrete production includes production of clinker, extraction of aggregates, transport to concrete plant, manufacturing the ready-mix concrete and associated usage of the plant. The boundaries for the construction process stage include all the processes from the manufacturing unit gate to the practical completion of the restoration task.

Module A1 refers to the extraction and production of raw materials.

Module A2 quantifies the environmental impacts of the transportation of raw materials to the manufacturing units.

Module A3 evaluates emissions due to product manufacturing process at the plant.

Module A4 normally includes the transportation of the materials and products from the factory gate to the construction site, as well as losses due to the transportation (e.g., products damaged or lost during transportation).

Module A5 is the construction and installation process and includes groundworks and landscaping, storage of product, transport of persons and construction equipment to and from the site, transport within the site, temporary works, on-site production, product transformation, provision of controlled environmental conditions during the construction process, ancillary materials not considered

in environmental product declarations (EPDs – e.g. formworks discarded at the end of the project), any intermediate disposal of wastes and transportation of waste during the construction and installation process (CEN, 2021).

In **Step 5** the resilience is quantified with focus on the structural capability of the asset to withstand a hazard occurrence based on a probabilistic assessment, by calculating the weighted capacity using the occurrence probabilities of different DS for a given IM, as per Eq. (4):

$$C(T = t) = \sum_{i=0}^{n} C(DS_i | T = t) \cdot P(DS = DS_i \mid IM) \tag{4}$$

where C(T = t) is the capacity of the asset at a given time t after the commencement of the restoration works, $C(DS_i | T = t)$ is the capacity of the asset for a given damage state (DS_i) at time t (see step 3 above) and $P(DS = DS_i \mid IM)$ is the probability of being in DS_i for a specific IM. Based on the fragility functions in step 2, this is given by Eq. (5), for i = 0 (no damage) to i = n (severe damage):

$$P(DS = DSi | IM) = P(DS \geqslant DS_i | IM) - P(DS \geqslant DS_{i+1} | IM) \tag{5}$$

C(t) defines the evolution of asset performance recovery, which is the resilience model. The area under this curve defines the resilience index (R) adapted by Cimellaro et al. (2009), for each recovery strategy j, considering a total of k alternative strategies (Eq. (6)).

$$R_j = \frac{1}{(t_h - t_e)} \int_{t_e}^{t_h} C(t) dt \tag{6}$$

where t_e is the time of the hazard occurrence that caused the damage, and t_h is the time for which is measured (see Fig. 1b).

Step 6, 7 and 8. This step optimises the metrics of resilience (R) and sustainability (S). Common optimisation methods can be used such as multicriteria decision making (MCDM), using e.g., Pareto fronts (Bocchini and Frangopol, 2012). A metric of cost C is also embedded in resilience. R is described in step 5, while below the description of S is given based on the tCO2e. For different restoration strategies, the tCO2e is given in Eq. (7).

$$tCO2e_j(T = t) = \sum_{i=0}^{n} tCO2e(DS_i | T = t) \cdot P(DS = DS_i | IM) \tag{7}$$

where $tCO2e_j(T = t)$ is the cumulative tCO2e of the asset under recovery at a given time t after the commencement of restoration. This is weighted based on the probability of the asset being in DS_i (Eq. (5)) and the temporal evolution of tCO2e per damage state, which depends on the emissions per restoration task (see step 4) and the sequence of restoration tasks (see case study below).

The maximum tCO2e for a number of k different restoration strategies at time t = t_h (end of recovery), is given by Eq. (8):

$$\max(tCO2e) = \max\left(\left\{tCO2e_j(T = t_h), : j = 1, \ldots, k\right\}\right) \tag{8}$$

Based on the above a new sustainability index (S) can be defined for a number of k alternative restoration strategies, see Eq. (9):

$$S_j = \frac{tCO2e_j(T = t_h)}{\max(tCO2e)} \tag{9}$$

The same rationale as per Eq. (7), Eq. (8), Eq. (9) is followed for the cost index C_j and the following equations is introduced for the estimation of C_j (Eq. (10)):

$$C_j = \frac{C_j(T = t_h)}{\max(C)} \tag{10}$$

where $C_j(T = t_h)$ is the total cost of restoration strategy j and max(C) is the maximum cost of all alternative strategies.

The metrics R_j, S_j, and C_j take values between 0 and 1. For R_j and S_j the maximum value is the optimum one, whereas for cost is the opposite.

For different climate projections, different restoration strategies and for a portfolio of transport assets, decision-making is facilitated on the basis of optimum resilience, sustainability and cost, considering the following practical global index:

$$I_{SRC,j} = \gamma_S \cdot S_j \cdot \frac{\gamma_R \cdot R_j}{\gamma_C \cdot C_j} \tag{11}$$

It is stressed that Eq. (11) represents an optimised solution from the point of view of S, R, and C. However, the sequence of restoration and prioritisation of critical asset recovery in a transport network after a disaster should account for accessibility to critical nodes, delays and traffic flows, centrality, and importance measures among others (Zamanifar and Hartmann, 2021; Zhang and Alipour, 2020).

4. Case study

The 3-span river-crossing bridge shown in Fig. 5a with shallow foundations was the reference bridge of this case study. The fragility

curves (Fig. 5b) and restoration models (Fig. 5c, Fig. 5d) were taken from Argyroudis and Mitoulis (2021) and Mitoulis et al. (2021), correspondingly, for four damage states (minor, moderate, extensive, severe). Nine scour depths ranging from 1.0 to 5.0 m with a step of 0.5 m were analysed. Only one pier foundation was considered to be scoured.

4.1. Quantification of resilience, sustainability, and cost

Regarding the quantification of **resilience**, this refers to the bridge capacity and how this performance parameter improves over time after the damage. This was calculated following step 5 of the framework by implementing Eq. (4) to Eq. (6) for each scour scenario. Fig. 6a illustrates the temporal evolution of the weighted bridge capacities, normalised with respect to the original capacity of the intact asset. The nine plots are divided into three sets of curves corresponding to low intensity (green lines), medium intensity (blue lines) and high intensity (red lines). The recovery time for the worst scenario is 230 days (time t_h in Eq. (6)). 95% of the capacity recovery is achieved on average after 70 days, 170 days and 190 days for the low, medium, and high hazard intensity, respectively. The area under these curves corresponds to the scenario-based resilience indexes. Fig. 6b illustrates the evolution of the resilience index R over time. The values R_{max} of Fig. 6b are the R_j when $t_h - t_e = 230$ days (Eq. (6)).

Regarding **sustainability**, a **baseline analysis** is carried out as per step 4 of the framework, in which the main materials, construction techniques and procedures using the mean time required for each restoration task are considered. For example, this includes in-situ concrete incorporating cement as the only binder, and newly produced reinforcing and prestressing rebars. The same strategies were analysed considering **low-carbon solutions**. This way the overall emissions for carbon-intensive tasks are minimised (CEN, 2012). This reduction is possible by replacing the materials from virgin sources with low-carbon materials and by using biofuel blends for the construction equipment. As a more sustainable alternative, the main conventional construction materials are replaced by low-carbon alternatives such as concrete in which cement is replaced by fly ash or GGBS in proportions of 25%, and steel rebars and tendons containing 97% recycled steel obtained through electric arc furnace production. The low-carbon alternatives provide a reduction in emissions of around 10% for concrete and 175% for steel per functional unit (Abdelmonim and Bompa, 2021). By replacing the conventional concrete, steel and mineral diesel with low-carbon concrete, recycled steel and biofuel, respectively, overall reductions of up to 50–60% are achieved for some restoration tasks (i.e. R16-18, R20-23). With low-carbon materials, tasks R17, R22 and R11 be associated with 438, 285 and 647 tCO2e, respectively. In terms of on-site activities, the baseline analysis assumes that the fuel is a 100% mineral diesel including well-to-tank and combustion at site emissions. The low-carbon alternative assumes a biofuel blend, which is associated with around 5% reductions in emissions. For all assessments it is assumed that the transportation distance for raw materials, concrete, steel, temporary works and construction equipment is 25 km and is performed by diesel articulated HGV (greater than3.5–33 t - average laden). Transportation of persons and construction machinery to and from the site are not accounted for and would count less than 1% of the total carbon emissions.

Fig. A1 of Appendix A illustrates the embodied carbon associated with each restoration task of the baseline analysis for all the restoration tasks considered. These are divided into three emission categories relating to materials, on-site activities, and transportation. Depending on the activities involved in the task, the materials can represent 21% to 99% of the total emissions of the task, with an average for all activities of 74%. On-site activities can represent between 2% and 100% of the total, whilst transportation up to around 6%. For some restoration tasks, these values are similar to those from the literature, which indicates that the construction activities would contribute 30% of the total, whilst transportation is around 4% or less.

As shown in Table A3, tasks that require a high amount of reusable temporary works and a low amount of new materials, such as tasks R1 to R4, have a balanced level of emissions between those associated with materials and those with equipment fuel consumption. In contrast, for tasks which require a high amount of materials such as concrete and reinforcements, the main emissions are associated with
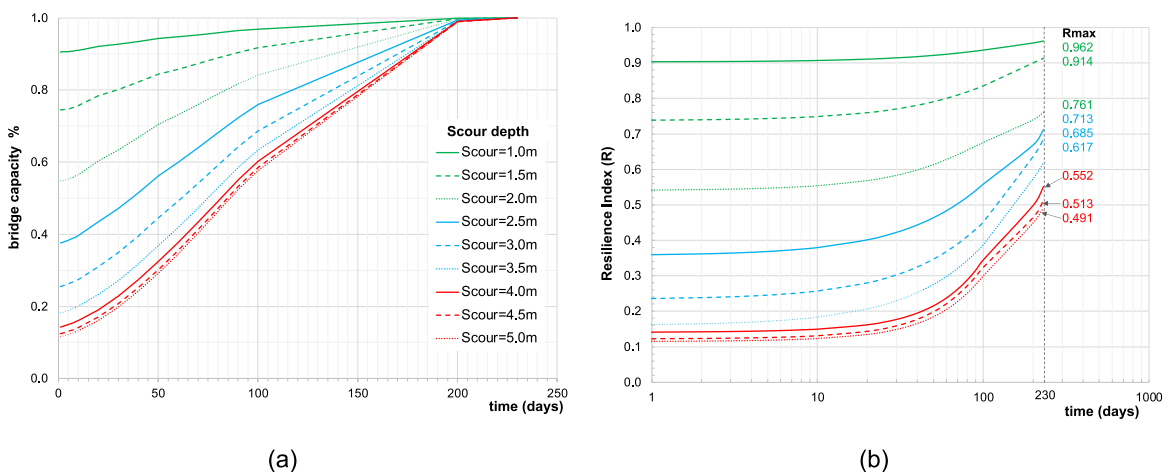

Fig. 6. (a) Resilience curves for bridge capacity and (b) evolution of the resilience index with time (right) for different scour depth scenarios (1.0 to 5.0 m).

the materials (e.g. R16-R19). This is also reflected in the total nominal values listed in Table A3. Tasks R17 (replacement of abutment and wingwalls), R22 (replacement of a deck span) and R11 (erosion protection measures) have the highest emissions per task, i.e. 947, 734 and 678 tCO2e, respectively. Unsurprisingly, the literature results indicate that the main carbon drivers are also tasks that utilize materials more heavily (Mackie et al., 2016). For example, up to around 80% of the total emissions are associated with materials extraction and production (Wang et al., 2015), which is very close to the average of the baseline analysis (i.e. 78%).

As mentioned above, both assessments incorporating conventional and low-carbon materials assumed the same mean duration for all restoration tasks and as a result, the resilience indexes of the alternative strategies (conventional and low carbon) did not differ. The latter is based on the assumption that the duration of all tasks is not affected by the application of low carbon materials and that low carbon materials are available from the same manufacturers that also provide the traditional materials. Shorter or longer duration of a task leads to reduced or increased on-site emissions, respectively, whilst the materials and transportation remain the same. To investigate the task duration influence on emissions, a sensitivity study in which the minimum and maximum durations by means of scalar factors are also carried out. Table A3 shows that a longer task for the construction activities and associated materials can lead to an increase in emissions by about 50% (R1). This is due to proportionally higher fuel consumption by construction equipment for the same output.

Fig. 7a and Fig. 7b illustrate the weighted tCO2e per DS and restoration task (R_i) considered in this case study as per Fig. 5d and the weighting factor of Table A2. Fig. 7a corresponds to the traditional restoration strategies, whereas Fig. 7b refers to the low carbon restoration approach (see Table A3). It is noted that for R23 the maximum values 1986 and 860 are given in the graphs, as these well exceed the max value of the tCO2e axis. It is observed that conventional and low carbon strategies have similar emissions for R1, R11, R12, R6, R2, R14, and R5, with differences up to 15%. For R16, R15 and R23 significant differences were observed ranging from 40%
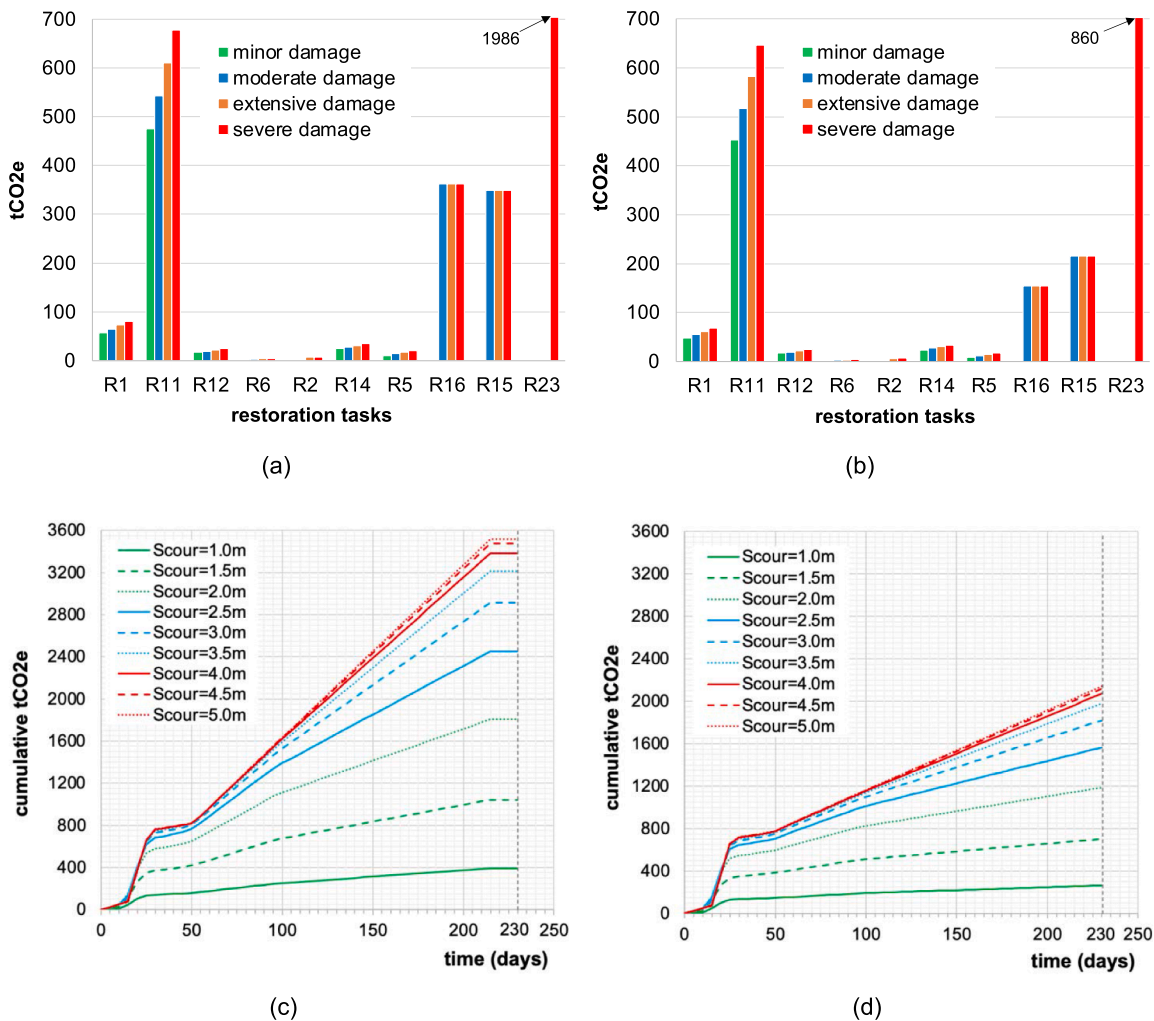

Fig. 7. Weighted tCO2e per damage state (see weights in Table A2) and restoration tasks (R_i) for (a) conventional restoration and (b) low carbon restoration (the order of the tasks is as per Fig. 5d). Evolution of cumulative weighted tCO2e (Eq. (7)) with time for conventional restoration (c) and low carbon restoration (d) for different scour depth scenarios (1.0 to 5.0 m).
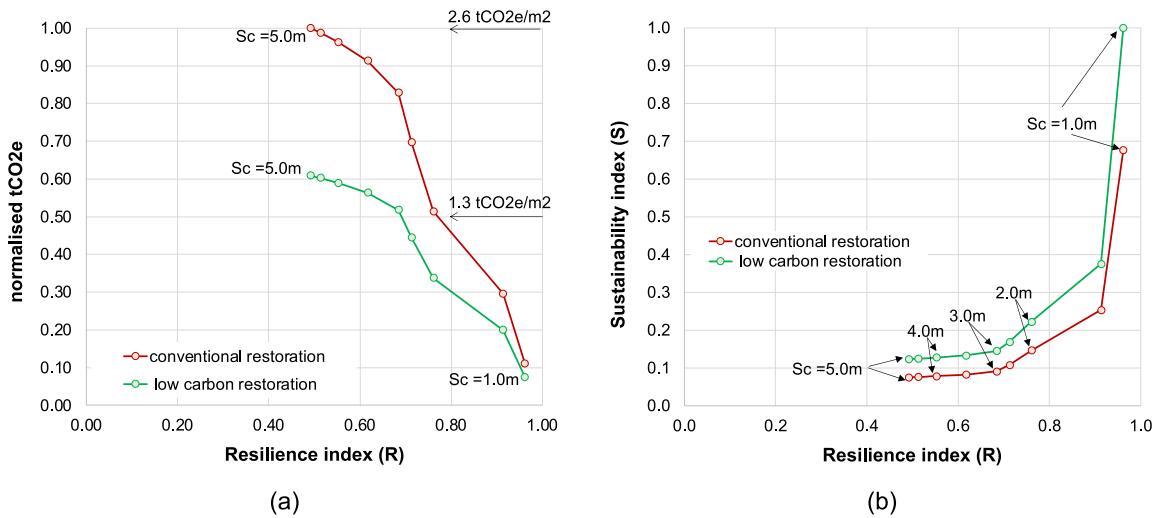
Fig. 8. (a) Normalised tCO2e vs. resilience index (R) and (b) sustainability index (S) vs. resilience index (R) for conventional restoration and low carbon restoration strategies for different scour depth scenarios (Sc = 1.0 to 5.0 m).
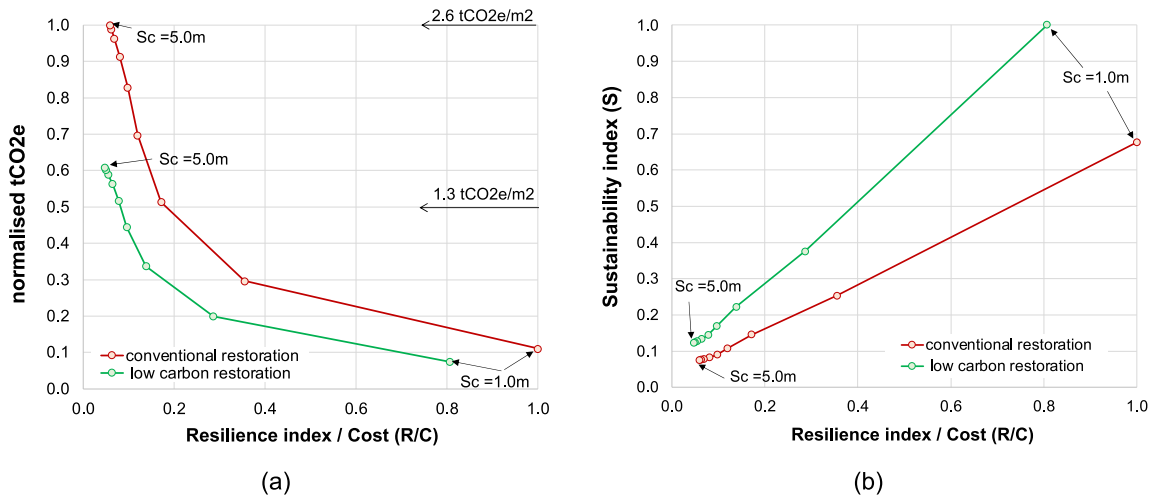

Fig. 9. (a) Normalised tCO2e vs. cost-based resilience index (R/C), (b) Sustainability index (S) vs. cost-based resilience index (R/C) of bridge damage restoration strategies for different scour depth scenarios (Sc = 1.0 to 5.0 m).

to 57%. The reason is that these tasks involved carbon-intense materials. Fig. 7c and Fig. 7d illustrate the evolution of cumulative weighted tCO2e for traditional restoration and more sustainable restoration strategies for different scour depth scenarios ranging from 1.0 to 5.0 m. The weighting was conducted based on Eq. (7). It was found that task R11, which includes erosion protection measures, is the most CO2-intensive task. This is shown by the abrupt change of the cumulative tCO2e from day 15 to 30 for all hazard scenarios. The second increase of cumulative tCO2e is observed at the time that R16 and R15 commence for moderate, extensive and severe damage.

In relation to the temporal scale of the restoration of the asset, the environmental impact of traffic diversion due to structure closure can be substantial (Steele et al., 2003). Depending on the project type, emissions due to diversions are up to 25% of the total project emissions (Noland and Hanson, 2015). These values are highly dependent on many conditions such as the volume of traffic, network layout and connectivity, alternative routes availability, as well as the timing of construction activities and closure times (Liu et al., 2019). Assessing these environmental impacts needs traffic simulations at both microscopic and mesoscopic levels (Sharifi et al., 2021; San José et al., 2021) which is outside the scope of this paper.

LCA results are highly sensitive to specific aspects of the life cycle inventory such as production methods, resource availability and regional context, among others, as well as the system boundaries and temporal scale. These are uncertainties that can influence the overall carbon emission outputs and can often result in conflicting outcomes (Santero and Horvath, 2009). For similar tasks, the results from this paper are with those available in the literature indicating the suitability of the adopted procedures for evaluating the environmental impact of bridge restoration in post-hazard conditions (Loijos et al., 2013; Wang et al., 2015; Liu et al., 2019).
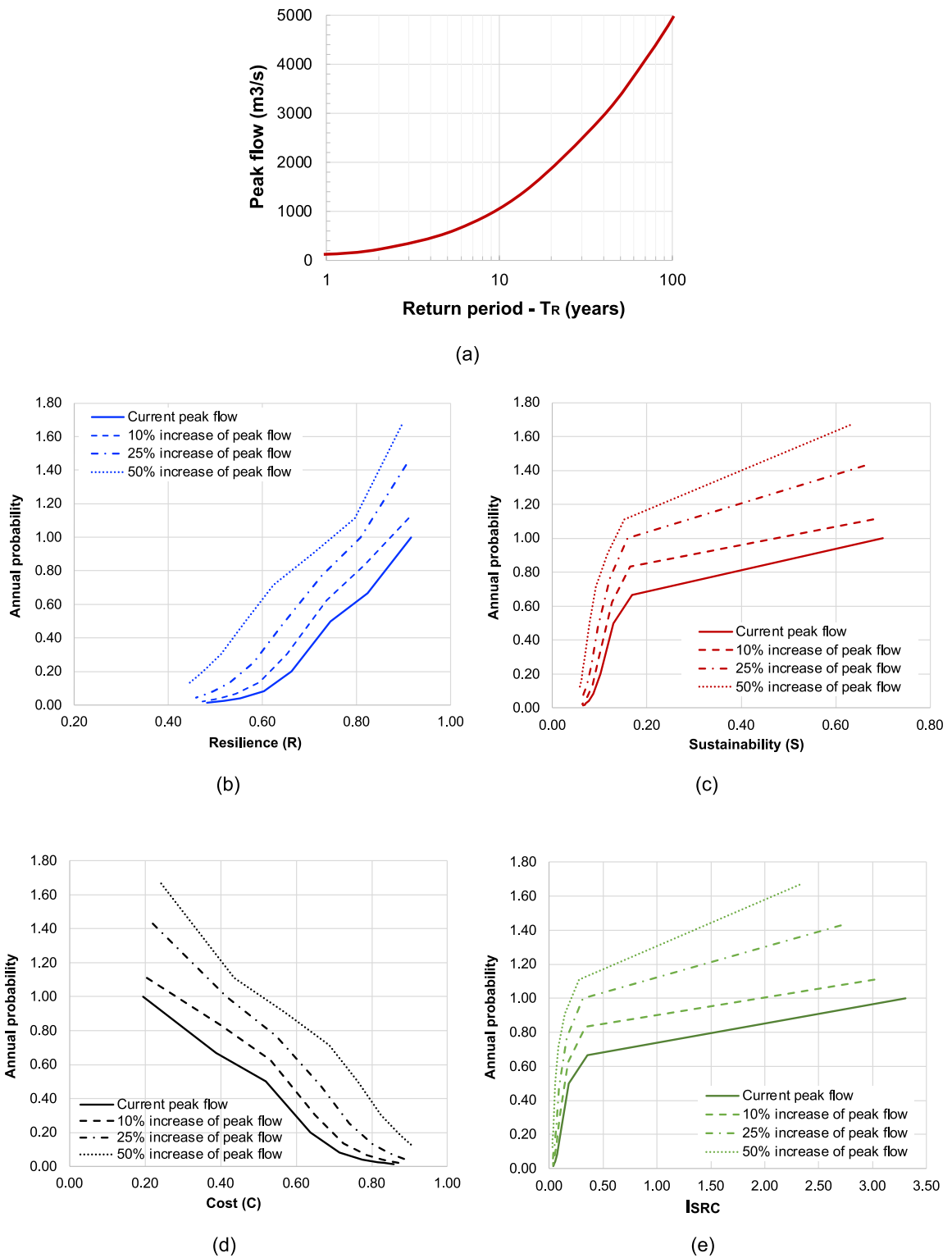
Fig. 10. (a) Hazard curve for the case study bridge - current peak flow vs return period. Normalised (b) resilience – R, (c) sustainability – S, (d) cost – C, (e) optimisation index – I_{SRC} vs. the annual probability of exceedance for current and increased peak flows (increased by 10%, 25%, 50%).

Table A1

Life cycle inventory.

Conversion factors	Unit	kgCO₂e per unit	Reference
Concrete - Insitu - C25/30 - CEM 1 - Not recommended	kg	0.142	Gibbons and Orr (2022)
Concrete - Insitu - UK C25/30 (25% GGBS)	kg	0.130	Gibbons and Orr (2022)
Steel - Rebar - Global avg	kg	2.289	Gibbons and Orr (2022)
Steel - Rebar - UK 97% recycled EAF production	kg	0.835	Gibbons and Orr (2022)
Stone	kg	0.138	Gibbons and Orr (2022)
Timber (sawn) - General	kg	0.587	Martínez-Alonso and Berdasco (2015)
Portland cement, CEM I	kg	0.860	The Concrete Centre (2020)
Mineral aggregate	kg	0.003	The Concrete Centre (2020)
Asphalt	kg	0.380	Hammond et al. (2011)
PVC pipe	kg	2.560	Hammond et al. (2011)
Fibreglass	kg	1.540	Hammond et al. (2011)
FRP	kg	5.000	Hammond et al. (2011)
Epoxy	kg	5.700	Hammond et al. (2011)
Rubber	kg	2.660	Hammond et al. (2011)
Bearings	kg	1.630	Smith et al. (2015)
Water supply	m3	0.344	BEIS (2021)
Diesel combustion (100% mineral diesel) WTT & Combustion at site*	litres	3.314	BEIS (2021)
Diesel (average biofuel blend) WTT & Combustion at site*	litres	3.156	BEIS (2021)
Electricity: UK	kWh	0.233	BEIS (2021)
Articulated diesel HGV (>3.5–33 t, average laden)	km	0.776	BEIS (2021)

* Main equipment consumption from manufacturer datasheets (l/h); RT Crane 45 T (18.2); Barge B < 20 m (6.0), JX Piling Rig (7.0) Cat 325 1.5 CY backhoe (23.2), Generic 5HP diesel water pump (0.80, Compressor Kaeser Honda G360 (6.0), Cat D7 Dozer (34.0), Asphalt mixer 16HP (9.2)

4.2. Results and discussion

In what is presented and discussed below, all values of cumulative tCO2e, sustainability index Sj, Resilience index Rj, and Cost index Cj, are normalised with respect to the maximum values observed for the scenarios analysed. This normalisation is useful if a portfolio of transport assets has to be assessed and prioritised on the same basis with the view of applying ex-ante adaptation or ex-post recovery. Fig. 8a illustrates the normalised tCO2e versus Resilience index R for the nine scenarios examined. The maximum value of cumulative (see Eq. (8)) 3516 or 2.6 tCO2e per m2 of the deck plan view area, was estimated for the conventional restoration strategy after a scour depth of Sc = 5.0 m was observed. All other estimates were normalised based on this value (Eq. (9)). The R index was calculated for all scenarios (see above). For scour depths up to 2.5 m the absolute values of cumulative tCO2e of the low carbon strategies are slightly smaller compared to the traditional strategies, but become more pronounced for higher hazard intensities (see e.g. Sc = 5.0 m), with increases up to 60%. Fig. 8b, shows that for the same R index the low carbon solution achieves higher S indexes. It is observed that when the scour depth is increased from 1.0 to 1.5 m the R index is reduced by approximately 5%, whereas the sustainability index is reduced from 1.0 to 0.38, which is a 62% reduction in the Sj. The significant difference between the R and S indexes reductions is due to the fact that the estimation of R assumes temporally overlapping tasks, while S takes into account the cumulative tCO2e of all tasks. The abrupt drop in S for a scour of 1.5 m is explained by the probabilities 0.433, 0.202, 0.124, 0.049 and 0.192 of the asset experiencing no, minor, moderate, extensive and severe damage correspondingly as per the fragility curves of Fig. 5b.

Based on the fact that R values are not affected by the use of conventional or low carbon restoration strategies, in all scenarios, the sustainable solutions were the optimum ones. To challenge this a cost-based resilience index R/C was introduced for all nine scenarios examined here. To this end, for the optimisation of sustainability and resilience, the cost of each Ri was increased based on evidence from the literature (see Table A4, Increase in materials cost). For example, the cost of low carbon concrete (aka green concrete) was found to be 20% higher than the conventional (Suhendro, 2014), while Muslemani et al. (2021) found that green steel is on average 25% more expensive than its conventional counterpart. This is reflected in the factors of 1.20 and 1.25. Likewise low carbon biofuel is expected to cost up to 50% more in comparison with fossil fuels, used for on-site activities and transportation. For the tasks that use less materials (e.g., R14, R20, R21), an adjustment factor of 1.05 was considered to be reasonable because carbon emissions are mainly induced by the materials. Finally, the cost of R11 and R12 was not affected when the low carbon strategy was assumed. Table A4 illustrates the increase in the total cost, which ranges between 8.9% for task R20 and 33.3% for R13. Fig. 9a compares the conventional and low carbon restoration strategies, based on the normalised tCO2e and the normalised cost-based resilience index (R/C) for the different scour depth scenarios. Despite the increase in the cost of the greener solutions up to 20%, the low carbon restoration strategy leads to a 50–60% reduction of the total tCO2e, which is a clear incentive for adopting more sustainable solutions. Similarly, the use of low carbon material appears to yield optimal solutions when S and R/C are plotted (see Fig. 9b). Nevertheless, it is observed that for a small increase of the scour depth from 1.0 to 1.5 m the cost-based resilience index was reduced by almost 64%, as opposed to the 5% of the R index, which demonstrates the importance of cost in understanding the trade-offs between sustainability and resilience. It is noted that the cost of tCO2 (tax) which has a value of approximately £20.51[3] represents approximately 1.6% and 0.8% of the total cost for the traditional and the low carbon solution, therefore it was considered to be negligible.

---

[3] https://www.statista.com/statistics/483590/prices-of-implemented-carbon-pricing-instruments-worldwide-by-select-country.

Table A2
Activities considered for the carbon assessments per restoration task R$_i$ and DS-specific weighting factors for task duration, tCO2e, and cost.

Restoration task (Ri)	Activities	Damage State specific weighting factors			
		Minor	Moderate	Extensive	Complete
R1 armouring countermeasures and flow-altering/cofferdam	Pre-dreging the site for the coffertam; driving the support piles install bracing; assume a cofferdam with a diameter of 35 m and UBP 305 × 305x 223 struts; assume all fuel related to on-site activities and consumable materials; the cofferdam/sheet piles and struts are temporary works and considered in carbon assessments	0.70	0.80	0.90	1.00
R2 temporary support per pier	Based on a load assessment, the temporary support structure would consist of two support frames incorporating UC 305 × 158 columns and UB 1016 × 305x 494 beams, and associated platforms; the assessments include some consumables, on-site installation and disassembly of the temporary support system, as well as the transportation of the temporary frames.	0.70	0.80	0.90	1.00
R3 temporary support of one abutment	The temporary structure would consist of similar frames as for R2 plus some struts and supplementary bracing, some consumables, on-site installation and disassembly of the temporary support system, as well as the transportation of the temporary frames.	0.70	0.80	0.90	1.00
R4 temporary support of one deck span /segment (midspan or support)	The temporary support structure would consist of a single support frame incorporating UC 305 × 158 columns and UB 1016 × 305x 494 beams, and associated platforms, assuming that the deck is still supported at one of the ends. The assessments include some consumables, on-site installation and disassembly of the temporary support, as well as the transportation of the temporary frames.	0.70	0.80	0.90	1.00
R5 repair cracks and spalling with epoxy and/or concrete	Scaffolding, removal of 50 mm of concrete with mechanical equipment and casting new concrete, resurfacing, new parapets, drainage pipes, associated consumables, on-site activities, transportation of materials, new concrete and demolition waste.	0.50	0.70	0.85	1.00
R6 re-alignment and/or levelling of pier	Assembly and disassembly of temporary support frames, scaffolding, associated consumables, transportation of materials, scaffolding and support frames.	0.50	0.70	0.85	1.00
R7 re-alignment of bearings	Assembly and disassembly of scaffolding, hydraulic press usage and associated consumables, transportation of materials, scaffolding and hydraulic jacks.	1.00	1.00	1.00	1.00
R8 jacketing or local strengthening (pier or abutment or foundation)	Partial removal of concrete, strengthening materials, scaffolding and transportation of new materials, demolition waste and scaffolding. Three alternatives considered: (i) grout repair and FRP, (ii) restoration using cement-based grout and steel reinforcement within a timber formwork, (iii) steel jacket and cement-based grout. It is assumed that the full pier is strengthened, rather than local jacketing. The strengthening detailing was chosen either based on common practice or through pre-sizing. FRP strengthening is considered as the default technology.	0.00	0.40	0.70	1.00
R9 jacketing or local strengthening (deck)	Strengthening materials, scaffolding and transportation of new materials, and scaffolding. Two suitable alternatives were considered: (i) FRP or (ii) steel jackets bolted with mechanical connectors. It is assumed that the entire bottom surface of the deck requires strengthening. The strengthening detailing was chosen either based on common practice or through pre-sizing. FRP strengthening is considered as the default technology.	0.00	0.40	0.70	1.00
R10 re-alignment of deck segment	The temporary structure would consist of similar frames as for R2 plus some struts and supplementary bracing, hydraulic press usage, some consumables, on-site installation and disassembly of the temporary support system, as well as the transportation of the materials, temporary frames, scaffolding and hydraulic jacks.	0.50	0.70	0.85	1.00
R11 erosion protection measures	Excavation, manufacturing and assembly of gabions, associated steel and stone materials. It is assumed that the intervention measures cover both riverbanks, both upstream and downstream for a 50 m length. Transportation of the materials as well as some transportation of excavated soil within the site is accounted for.	0.70	0.80	0.90	1.00
R12 rip-rap and/or gabions for filling of scour hole and scour protection	Compaction of the riverbed, placement and compaction of the rip-rap within the scour hole to the river bed zero ground. The scour holes size was considered for moderate damage conditions and was assumed having a depth of 2.5 m and a diameter of 7.75 m. Transportation of the materials as well as some transportation of excavated soil within the site is accounted for.	0.70	0.80	0.90	1.00
R13 removal of debris	Energy associated debris removal activities	0.70	0.80	0.90	1.00
R14 ground improvement per foundation	Excavation around the foundation, installation of a 2 m deep compacted gravel layer, associated materials and consumables. A	0.70	0.80	0.90	1.00

Table A2 (*continued*)

Restoration task (Ri)	Activities	Damage State specific weighting factors			
		Minor	Moderate	Extensive	Complete
R15 installation of deep foundation system	support system as for R2 is accounted for Transportation of the new materials and temporary support system considered. Assumed a group of 16 piles of 800 mm diameter and a pile cap of $3.5 \times 5.5 \times 1.5$ m made of reinforced concrete with a gross longitudinal reinforcement ratio of 4%. The assessment includes all materials, consumables, associated on-site activities, and transportation of the materials and temporary support frames.	1.00	1.00	1.00	1.00
R16 extension of foundation footing	It is assumed that the footing is extended on all sides by 2 m over a depth of 1.5 m. The assessment includes some concrete removal from the existing structure, formwork, the steel reinforcement and the concrete and associated construction activities. Transportation of the materials, consumables and waste concrete is included.	1.00	1.00	1.00	1.00
R17 reconstruction/replacement of the abutment and wingwalls	Temporary support of the deck and scaffolding, removal of the approach slab, excavation of the soil adjacent to the existing abutment and wing walls, demolition of the existing abutment and wing walls, installation of formwork, reinforcement and concrete, placement and compaction of soil. The assessment includes all materials, consumables and transportation of the new materials, scaffolding, temporary support, and the demolished concrete.	1.00	1.00	1.00	1.00
R18 reconstruction/replacement of the pier	Temporary support of the decks and scaffolding, demolition of the existing pier, installation of formwork, reinforcement and concrete. The assessment includes all materials, associated consumables and transportation of the new materials, scaffolding, temporary support frames, and the demolished concrete waste.	1.00	1.00	1.00	1.00
R19 temporary support and replacement of the bearings	Assembly and disassembly of scaffolding and temporary support frames, hydraulic press usage and associated consumables, transportation of materials, scaffolding, support frames and hydraulic jacks.	1.00	1.00	1.00	1.00
R20 replacement of the backfill and approach slab and mudjacking	Removal of the approach slab, excavation over a 2 m depth after removal of the slab, placement and compaction of new soil, installation of formwork, reinforcement and concrete. The assessment includes all materials, associated consumables and transportation of the new materials, scaffolding, temporary support frames, and the demolition waste	1.00	1.00	1.00	1.00
R21 replacement of expansion joint	Removal of the existing expansion joint and of the pavement 1 m each side of the joint. Installation of a new expansion joint and resurfacing. Materials and transportation are included.	0.50	0.70	0.85	1.00
R22 demolish/replacement of a deck span/segment	Demolition of the existing deck and the installation of the new box girder. The fabrication and installation of the deck segments includes reinforcing and prestressing steel, concrete, as well cast in situ materials. Transportation of the main materials and of the launching gantry is included.	1.00	1.00	1.00	1.00
R23 demolish/replacement (part) of the bridge	Only for comparative measures, assuming that one span is not affected, for this study it is assumed that a pier, and two decks are being replaced. Hence, the activities described in R1, R18, 19 and R22 are considered.	1.00	1.00	1.00	1.00

4.3. Impact of climate change on sustainability and resilience in transport asset recovery

In this section, the impact of climate change on the optimised I_{SRC}, as well as on the individual metrics of sustainability – S, resilience – R and cost – C, are investigated. For the case study bridge, data from the UKCP18 probabilistic projections were employed for a realistic riverine bridge location (River Falloch in Scotland), to demonstrate the impact of RCP8.5, as per Appendix C, Table 6 in Sayers et al. (2020). This table provides the change in the return period, for a given increase (percentage change) in the peak flow for fluvial flooding as a consequence of climate change. For example, if based on a climate projection, a 10% increase is estimated for the peak flow (+10%) this would reduce the return period of the intensity measure (e.g. peak flow discharge) from 1:10 (current) to 1:6.2 years (future projection). Hence, the annual probability would be increased from 0.1 to 0.16. This, in conjunction with Eq. (1), for a given lifespan of an asset, e.g., 100 years for a bridge, the exceedance probability P_R can be estimated.

For the case study, a realistic hazard curve (peak flow vs return period) shown in Fig. 10a was used. In this application the scour depth, which was used as the intensity measure for the hazard scenarios (1.0 to 5.0 m), was linked to the water peak flow discharge based on closed-form solutions provided by Arneson et al. (2012). The peak flow ranges from 20 m^3/s to 5000 m^3/s corresponding to scour depths of 1.22 m to 4.93 m, for a channel width of 35 m, and hence one pier is founded in the riverbed. The current peak flow discharges described above will lead to reduced R, S and increased C when the annual probability reduces, i.e., when more rare hazard occurrences are expected. As a result, the optimised I_{SRC} will also be reduced.

Table A3
Carbon assessments.

No	Action type	Conventional materials (mean values of tCO2e)				Low carbon solution (1) (3) (4)	Influence of duration(2)
		Materials	On-site activities	Trans-portation	Total	%	%
R1	armouring countermeasures and flow-altering/cofferdam	16.9	63.6	0.1	80.6	−14.9	±49.8
R2	temporary support per pier	2.7	4.9	0.1	7.7	−9.6	±30.6
R3	temporary support of one abutment	3.1	6.3	0.2	9.7	−9.9	±35.3
R4	temporary support of one deck span /segment (midspan or support)	1.6	2.4	0.1	4.1	−9.2	±29.8
R5	repair cracks and spalling with epoxy and/or concrete	18.3	1.1	1.2	20.6	−17.6	±3.8
R6	re-alignment and/or levelling of pier	3.4	0.7	0.1	4.2	−13.4	±7.5
R7	re-alignment of bearings	1.1	0.6	0.0	1.7	−4.8	±19.1
R8	jacketing or local strengthening (pier or abutment or foundation)	2.6	0.4	0.0	3.0	−7.3	±6.1
R9	jacketing or local strengthening (deck)	2.7	0.3	0.0	3.0	−0.4	±3.7
R10	re-alignment of deck segment	4.2	4.9	0.1	9.2	−10.3	±20.2
R11	erosion protection measures	645.5	29.0	3.5	678.0	−4.6	±1.7
R12	rip-rap and/or gabions for filling of scour hole and scour protection	21.7	2.5	0.1	24.3	−1.0	±6.1
R13	removal of debris	0.0	0.4	0.0	0.4	−4.8	±44.2
R14	ground improvement per foundation	29.0	5.0	0.3	34.3	−1.3	±7.0
R15	installation of deep foundation system	235.0	113.9	0.4	349.2	−38.3	±10.5
R16	extension of foundation footing	346.5	16.2	0.2	362.9	−57.4	±1.7
R17	reconstruction/replacement of the abutment and wingwalls	902.0	43.2	1.7	946.9	−53.7	±1.8
R18	reconstruction/replacement of the pier	382.6	6.7	0.8	390.2	−54.8	±0.5
R19	temporary support and replacement of the bearings	11.2	0.5	0.2	11.9	−4.5	±1.9
R20	replacement of the backfill and approach slab and mudjacking	82.1	1.8	0.1	84.0	−54.9	±1.0
R21	replacement of expansion joint	34.6	0.0	0.0	34.6	−63.5	0.0
R22	demolish/replacement of a deck span/segment	711.4	20.1	2.1	733.5	−61.2	−1.1
R23	demolish/replacement (part) of the bridge	1867.1	112.8	5.7	1985.6	−56.7	−3.3

(1) replacement of main construction materials and fuel with low-carbon alternatives as described in Section 4.1 (see sustainability and low-carbon solution).

(2) increase/decrease of carbon corresponding to the use of onsite equipment and machinery (due to uncertainty in the recovery task duration, see Table 3 in Mitoulis et al., 2021), e.g. for R1 it was assumed that for 63.6 tCO2e are emitted in 15.2 days (mean); whilst an in/decrease of +/- 49.8% of the total emissions will occur if the period is shortened/extended by 13.4 days. Emissions associated with materials and transportation (of materials, temporary works, etc) do not influence the emissions associated with on-site activities (these are outside of the 'construction stage' module).

(3) R8 – replacement of (i) FRP strengthening with ii) cement-based grout and steel reinforcement within a timber formwork increased the total carbon emissions to 20.7 tCO2e, and with iii) steel jacket and cement-based grout to 18.40 tCO2e (see Table A2 for details).

(4) R9 – replacement of FRP strengthening with steel jackets bolted with mechanical connectors, increased the total carbon emissions to 182.95 tCO2e (see Table A2 for details).

Apart from the current hazard (Fig. 10a), a further three exacerbations of peak flow discharge were examined corresponding to an increase of 10%, 25% and 50% due to climate change. The results are shown in Fig. 10b to Fig. 10e, which illustrate the annual probability of exceedance, for the three metrics, i.e., S, R, C, and the global metric I_{SRC}. When the peak flow increases due to climate exacerbations of the hazard, the metrics of R, S and I_{SRC} will be reduced, and the cost C will be increased. For example, an increase of 25% of the peak flow, will reduce the annual probability of 0.1 the S and R by 24% and 17%, while the C will be increased by 17%, leading to a decrease of the I_{SRC} by 46%. For more frequent events, e.g., event characterised by an annual probability of 1.0, the S and R will be reduced by 77% and 12%, while the C will be increased by 113%, leading to a decrease of I_{SRC} by 91%. This result justifies ex-ante adaptation measures for more frequent flood events. The significant drop of S and I_{SRC} and increase of C, were explained in Fig. 8b and Fig. 9b. The scenario-based analysis is a demonstration of how resilience, sustainability and cost can be integrated and streamlined into operators' decision-making in one index (I_{SRC}) to justify both ex-ante adaptation and ex-post recovery strategies, in transport infrastructure maintenance. For example, the design objective of transport operators could be to either maintain an reasonable level of I_{SRC} throughout the lifespan of the asset and/or prioritise climate adaptation of assets based on normalised I_{SRC}.

5. Conclusions

A novel framework for quantifying the trade-offs between sustainability (S) and resilience (R) was introduced and applied to a critical transport asset - a bridge - toward a comprehensive assessment of the performance and cost (C) of transport infrastructure. The framework introduced an integrated index, I_{SRC}, which can be used to appraise the impact of climate projections on adaptation strategies that take into account climate resilience, a sustainability metric i.e., the tCO2e, and the cost of restoration/adaptation tasks

Table A4

Cost of materials, on-site activities and transportation for each restoration task Ri.

	Conventional				Low carbon		
	Materials (£)	On-site activities (£)	Transportation (£)	Total (£)	Increase in materials cost	Total (£)	Cost increase
R1	45,971	32,436	12,420	90,828	1.20	122,449	25.8%
R2	17,132	2,488	12,420	32,041	1.25	43,777	26.8%
R3	19,269	3,235	15,525	38,029	1.25	52,226	27.2%
R4	10,448	1,244	6,210	17,902	1.25	24,241	26.1%
R5	130,734	616	94,703	226,052	1.20	299,859	24.6%
R6	1,450	1,259	12,420	15,128	1.25	22,331	32.3%
R7	8,593	292	1,553	10,437	1.25	13,509	22.7%
R8	31,308	162	4,658	36,127	1.25	46,365	22.1%
R9	135,289	137	1,553	136,979	1.25	171,646	20.2%
R10	26,970	2,488	217,351	246,809	1.25	363,471	32.1%
R11	518,598	14,764	281,003	814,365	1.00	962,249	15.4%
R12	16,179	1,284	10,868	28,331	1.00	34,407	17.7%
R13	–	–	224	224	1.00	336	33.3%
R14	21,771	2,545	24,840	49,156	1.05	63,937	23.1%
R15	346,174	52,327	32,603	431,104	1.20	542,804	20.6%
R16	539,452	9,591	20,183	569,226	1.20	692,003	17.7%
R17	2,264,558	24,988	139,725	2,429,271	1.20	2,964,539	18.1%
R18	976,214	3,612	66,758	1,046,583	1.20	1,277,012	18.0%
R19	93,030	292	12,420	105,742	1.25	135,356	21.9%
R20	122,159	1,942	12,420	136,522	1.05	149,810	8.9%
R21	2,179	1	1,553	3,733	1.25	5,055	26.1%
R22	114,718	10,258	167,670	292,646	1.20	404,554	27.7%
R23	1,623,742	57,731	464,199	2,145,671	1.20	2,731,385	21.4%

The costs are based on the same quantities used for assessment of carbon emissions depicted in Table A1. The costs were assessed based on the 2018 rates for Building, Civil Engineering and Highway Works (AECOM, 2018a; AECOM, 2018b), and modified using the UK Gov Price Indices from the Monthly Bulletin of Building Materials and Components, May 2022, No. 567 (BEIS, 2022). These do not include costs due to disposal of waste and other site materials, land taxes, manufacturing and materials for temporary works, labour, overheads.
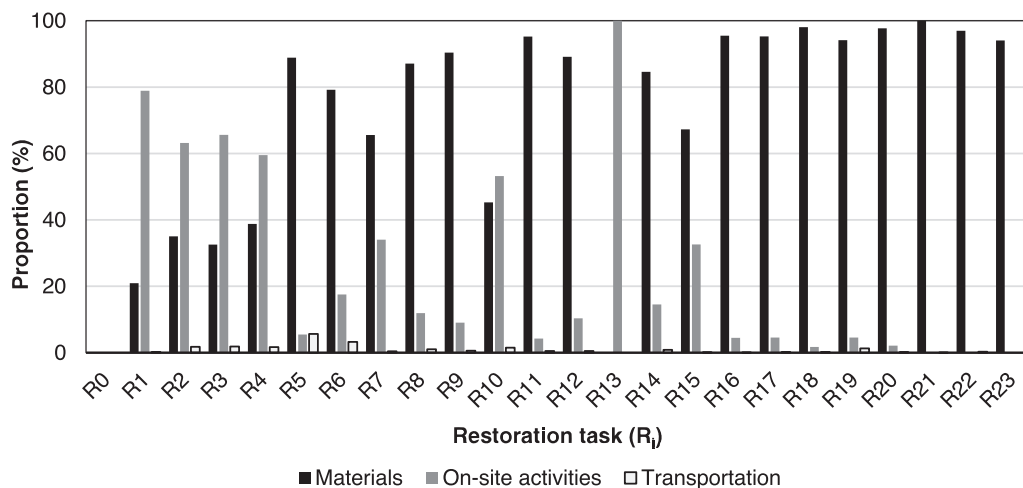

Fig. A1. Environmental impact (tCO2e proportion %) due to materials use, on-site procedures and transportation for each restoration task (R_i).

in transport assets affected by floods. The framework can be tailored and made applicable to other infrastructure assets, and for the prioritisation in post-disaster rehabilitation of transport networks. For the quantification of resilience, sustainability and cost, fragility and restoration models were deployed, and a probabilistic approach was adopted for different hazard scenarios. For all metrics, the sequence and duration of restoration tasks were considered. Conventional and low-carbon restoration strategies were compared based on normalised metrics of sustainability (S), resilience (R) and cost (C). The application of the framework, on a river-crossing bridge considering nine flood scenarios, led to the following conclusions:

- Sustainability and resilience can be synergistic, independent, or competing design targets. It was found that in bridge post-flood restoration, sustainability and resilience are less dependent, while the former competes with cost. In all scenarios examined in this paper, the application of a low carbon restoration strategy, which reduces substantially the tCO2e due to the use of low carbon materials, on-site activities, and transportation, resulted in up to 50% higher I_{SRC}. This can justify the additional investments for introducing greener adaptation strategies in transport infrastructure.
- An abrupt loss of performance in terms of optimised sustainability and resilience was observed at low intensities of the hazard, mainly owed to the significant increase of tCO2e due to the additional carbon-intensive tasks required for the restoration of the asset after the flood. This demonstrates the impact of carbon-intensive preparatory restoration tasks, in this case corresponding to R11 (erosion protection measures), which is required in all scenarios and damage states. Instead, resilience was not dramatically reduced at the lower intensity of the hazard because resilience mainly depends on the duration of the tasks, which overlap in most restoration scenarios.
- The integrated index I_{SRC} can be used for informed decision making, incorporating the principles of resilience, sustainability, and cost to adapt transport systems to climate change. To this end, the annual probabilities for the S, R and C metrics were calculated considering current and increased due to climate change hazard intensities by 10%, 25% and 50%. This led to substantial reductions in I_{SRC}, which were more pronounced at lower values of the intensity measure (scour). This optimisation index can be used to combine the design objectives of S, R, and C in asset management and calibrate its adaptive capacity throughout its lifespan, based on a practical starting point. Likewise, the same can be used to prioritise recovery strategies of portfolios of assets using normalised I_{SRC}.

Regarding future research in this area, it is suggested that enhanced LCAs suitable for transportation assets, could include: (a) traffic diversion modelling, (b) accounting for benefits from recycling and reusing materials from demolition within restoration tasks, (c) emissions offsetting due to environment-positive interventions, e.g. solar panels, carbon sequestration, concrete carbonation, (d) uncertainty modelling using established approaches (Monte Carlo, ML, AI) (Tsakalidis et al., 2020), and (e) two-way communication with Building Information Model (BIM) models and Digital-Twins for enhancing sustainability and climate resilience assessments (Argyroudis et al., 2022).

Declaration of Competing Interest

The authors declare that they have no known competing financial interests or personal relationships that could have appeared to influence the work reported in this paper.

Appendix A

Tables A1 to A4 show estimates of carbon emissions for the restoration tasks described in Mitoulis et al. (2021).Fig. A1

References

Abdelmonim, A., Bompa, D.V., 2021. Mechanical and Fresh Properties of Multi-Binder Geopolymer Mortars Incorporating Recycled Rubber Particles. Infrastructures 6 (10), 146. https://doi.org/10.3390/infrastructures6100146.
Achilleos, C., Hadjimitsis, D., Neocleous, K., Pilakoutas, K., Neophytou, P.O., Kallis, S., 2011. Proportioning of steel fibre reinforced concrete mixes for pavement construction and their impact on environment and cost. Sustainability 3 (7), 965–983. https://doi.org/10.3390/su3070965.
AECOM, 2018a. Spon's Civil Engineering and Highway Works Price Book, 32nd ed. CRC Press.
AECOM, 2018b. Spon's Architects' and Builders' Price Book 2018, 1st ed. CRC Press.
Alipour, A., Shafei, B., 2016. Seismic resilience of transportation networks with deteriorating components. J. Struct. Eng. 142 (8), C4015015.
Argyroudis, S.A., Mitoulis, S.A., 2021. Vulnerability of bridges to individual and multiple hazards-floods and earthquakes. Reliab. Eng. Syst. Saf. 210, 107564.
Argyroudis, S.A., Mitoulis, S.A., Winter, M.G., Kaynia, A.M., 2019. Fragility of transport assets exposed to multiple hazards: State-of-the-art review toward infrastructural resilience. Reliab. Eng. Syst. Saf. 191, 106567.
Argyroudis, S.A., Mitoulis, S.A., Hofer, L., Zanini, M.A., Tubaldi, E., Frangopol, D.M., 2020. Resilience assessment framework for critical infrastructure in a multi-hazard environment: Case study on transport assets. Sci. Total Environ. 714, 136854.
Argyroudis, S.A., Mitoulis, S.A., Chatzi, E., Baker, J.W., Brilakis, I., Gkoumas, K., Vousdoukas, M., Hynes, W., Carluccio, S., Keou, O., Frangopol, D.M., Linkov, I., 2022. Digital technologies can enhance climate resilience of critical infrastructure. Clim. Risk Manag. 35, 100387.

Argyroudis, S.A., 2021. Resilience metrics for transport networks: a review and practical examples for bridges. In Proceedings of the Institution of Civil Engineers-Bridge Engineering (pp. 1-14).

Arneson L.A., Zevenbergen L.W., Lagasse P.F., Clopper P.E., 2012. Evaluating scour at bridges. Hydraulic Engineering Circular (HEC) No. 18, Publication No. FHWA-HIF-12-003, Washington, DC.

ASCE Report Card History (2021). Report Card for America's Infrastructure, https://infrastructurereportcard.org/making-the-grade/report-card-history, accessed May 16, 2022.

Barandica, J.M., Fernández-Sánchez, G., Berzosa, Á., Delgado, J.A., Acosta, F.J., 2013. Applying life cycle thinking to reduce greenhouse gas emissions from road projects. J. Clean. Prod. 57, 79–91. https://doi.org/10.1016/j.jclepro.2013.05.036.

BEIS (Department for Business, Energy and Industrial Strategy) (2021). Government Greenhouse Gas Conversion Factors for Company Reporting Methodology Paper for Conversion factors Final Report. UK Gov. Report Online. Available at: https://assets.publishing.service.gov.uk/government/uploads/system/uploads/attachment_data/file/1049346/2021-ghg-conversion-factors-methodology.pdf [accessed 1 May 2022].

BEIS (Department for Business, Energy & Industrial Strategy) (2022). Monthly Bulletin of Building Materials and Components - May 2022 No. 567. Online. Available at: https://www.gov.uk/government/statistics/building-materials-and-components-statistics-may-2022 [accessed 1 June 2022].

Bocchini, P., Frangopol, D.M., 2012. Optimal resilience-and cost-based postdisaster intervention prioritization for bridges along a highway segment. J. Bridg. Eng. 17 (1), 117–129.

Bocchini, P., Frangopol, D.M., Ummenhofer, T., Zinke, T., 2014. Resilience and sustainability of civil infrastructure: Toward a unified approach. J. Infrastruct. Syst. 20 (2), 04014004.

Bruneau, M., Chang, S.E., Eguchi, R.T., et al., 2003. A framework to quantitatively assess and enhance the seismic resilience of communities. Earthq. Spectra 19 (4), 733–752.

CEN (European Committee for Standardization), 2005. Eurocode 8: Design of structures for earthquake resistance-part 1: general rules, seismic actions and rules for buildings. Brussels: European Committee for Standardization.

CEN (European Committee for Standardization), 2012. EN 15804:2012. Sustainability of construction works. Environmental product declarations. Core rules for the product category of construction products. CEN, Brussels, Belgium.

CEN (European Committee for Standardization), 2021. EN 17680. Sustainability of construction works. Evaluation of the potential for sustainable refurbishment of buildings. CEN, Brussels, Belgium.

CEN (European Committee for Standardization), 2022. EN 17472:2022 (E) Sustainability of construction works - Sustainability assessment of civil engineering works - Calculation methods. CEN, Brussels, Belgium.

Cimellaro, G.P, Fumo, C, Reinhorn, A.M., Bruneau, M., 2009. Quantification of disaster resilience of health care facilities. Technical Report MCEER-09-0009, Buffalo, NY.

Dong, Y., Frangopol, D.M., Saydam, D., 2013. Time-variant sustainability assessment of seismically vulnerable bridges subjected to multiple hazards. Earthq. Eng. Struct. Dyn. 42 (10), 1451–1467. https://doi.org/10.1002/eqe.2281.

Dong, Y., Frangopol, D.M., Saydam, D., 2014. Sustainability of highway bridge networks under seismic hazard. J. Earthq. Eng. 18 (1), 41–66. https://doi.org/10.1080/13632469.2013.841600.

European Commission, 2019. The European Green Deal, COM(2019) 640 final, online available at: https://ec.europa.eu/info/sites/default/files/european-green-deal-communication_en.pdf.

Frangopol, D.M., Dong, Y., Sabatino, S., 2017. Bridge life-cycle performance and cost: analysis, prediction, optimisation and decision-making. Struct. Infrastruct. Eng. 13 (10), 1239–1257.

Gibbons, O.P., Orr, J.J., 2022. How to calculate embodied carbon, second ed. IStructE Ltd.

Hammond, G., Jones, C., Lowrie, E.F., Tse, P., 2011. Embodied carbon. The inventory of carbon and energy (ICE). Version (2.0). BSRIA, UK.

Haraguchi, M., Lall, U., 2015. Flood risks and impacts: A case study of Thailand's floods in 2011 and research questions for supply chain decision making. Int. J. Disaster Risk Reduct. 14, 256–272.

Heidari, M.R., Heravi, G., Esmaeeli, A.N., 2020. Integrating life-cycle assessment and life-cycle cost analysis to select sustainable pavement: A probabilistic model using managerial flexibilities. J. Clean. Prod. 254, 120046 https://doi.org/10.1016/j.jclepro.2020.120046.

Horvath, A., 2005. Decision-making in Electricity Generation Based on Global Warming Potential and Life-cycle Assessment for Climate Change. Final report, (UCEI) Energy Policy and Economics Working Paper Series, UC Berkeley: University of California Energy Institute, Berkeley, CA, USA, 15 pp.

IPCC (Intergovernmental Panel on Climate Change), 2021. AR6 Climate Change 2021: The Physical Science Basis. Geneva, Switzerland. Online. Available at https://www.ipcc.ch/report/ar6/wg1/ [accessed 1 May 2022].

ISO (International Organization for Standardization), 2006. ISO 14044:2006 Environmental management — Life cycle assessment — Requirements and guidelines. Geneva, Switzerland.

Jiang, R., Wu, P., 2019. Estimation of environmental impacts of roads through life cycle assessment: A critical review and future directions. Transp. Res. Part D: Transp. Environ. 77, 148–163. https://doi.org/10.1016/j.trd.2019.10.010.

Karamlou, A., Bocchini, P., 2017. From component damage to system-level probabilistic restoration functions for a damaged bridge. J. Infrastruct. Syst. 23 (3), 04016042.

Kay, A.L., Rudd, A.C., Fry, M., Nash, G., Allen, S., 2021. Climate change impacts on peak river flows: Combining national-scale hydrological modelling and probabilistic projections. Clim. Risk Manag. 31, 100263.

Keoleian, G.A., Kendall, A., Dettling, J.E., Smith, V.M., Chandler, R.F., Lepech, M.D., Li, V.C., 2005. Life cycle modeling of concrete bridge design: Comparison of engineered cementitious composite link slabs and conventional steel expansion joints. J. Infrastruct. Syst. 11 (1), 51–60. https://doi.org/10.1061/(ASCE)1076-0342(2005)11:1(51).

Khanna, N., Wadhwa, J., Pitroda, A., Shah, P., Schoop, J., Sarıkaya, M., 2022. Life cycle assessment of environmentally friendly initiatives for sustainable machining: A short review of current knowledge and a case study. Sustainable. Mater. Technol. e00413.

Liu, Y., Wang, Y., Li, D., Yu, Q., 2019. Life cycle assessment for carbon dioxide emissions from freeway construction in mountainous area: Primary source, cut-off determination of system boundary. Resour. Conserv. Recycl. 140, 36–44. https://doi.org/10.1016/j.resconrec.2018.09.009.

Loijos, A., Santero, N., Ochsendorf, J., 2013. Life cycle climate impacts of the US concrete pavement network. Resour. Conserv. Recycl. 72, 76–83. https://doi.org/10.1016/j.resconrec.2012.12.014.

Loli, M., Mitoulis, S.A., Tsatsis, A., Manousakis, J., Kourkoulis, R., Zekkos, D., 2022. Flood characterization based on forensic analysis of bridge collapse using UAV reconnaissance and CFD simulations. Sci. Total Environ. 822, 153661.

Lounis, Z., McAllister, T. P., 2016. Risk-based decision making for sustainable and resilient infrastructure systems. Journal of Structural Engineering, 142(9), F4016005. p. doi: 10.1061/(ASCE)ST.1943-541X.0001545.

Mackie, K.R., Kucukvar, M., Tatari, O., Elgamal, A., 2016. Sustainability metrics for performance-based seismic bridge response. J. Struct. Eng. 142 (8), C4015001. https://doi.org/10.1061/(ASCE)ST.1943-541X.0001287.

Marchese, D., Reynolds, E., Bates, M.E., Morgan, H., Clark, S.S., Linkov, I., 2018. Resilience and sustainability: Similarities and differences in environmental management applications. Sci. Total Environ. 613, 1275–1283.

Marriott, D., Pampanin, S., Palermo, A., 2009. Quasi-static and pseudo-dynamic testing of unbonded post-tensioned rocking bridge piers with external replaceable dissipaters. Earthquake Eng. Struct. Dyn. 38(3), 331-354.

Martínez-Alonso, C., Berdasco, L., 2015. Carbon footprint of sawn timber products of Castanea sativa Mill. in the north of Spain. J. Clean. Prod. 102, 127–135.

Maxineasa, S.G., Neocleous, K., Dumitrescu, L., Themistocleous, K., Taranu, N., Hadjimitsis, D.G., 2017. Environmental LCA of innovative reuse of all End-of-life tyre components in concrete. Proceedings of the 1st International Conference on Construction Materials for Sustainable Future, Zadar, Croatia, 19 - 21 April 2017.

McKenna, G., Argyroudis, S.A., Winter, M.G., Mitoulis, S.A., 2021. Multiple hazard fragility analysis for granular highway embankments: Moisture ingress and scour. Transp. Geotech. 26, 100431.

Michaels, B., 2007. Intermodal container transfer facility modernization project. Union Pacific Railroad. Joint Powers Authority. Report. Online. Available at: http://ictf-jpa.org/document_library/application_development_project_approval/Final%20ICTF%20ADPA%2012-22-2007.pdf [accessed 1 May 2022].

Mitoulis, S.A., 2020. Challenges and opportunities for the application of integral abutment bridges in earthquake-prone areas: A review. Soil Dyn. Earthq. Eng. 135, 106183.

Mitoulis SA, Domaneschi M, Cimellaro G-P, Casas J-R, 2021. Bridge and transport network resilience – a perspective, ICE – Bridge Engineering -Themed Issue on Bridge and transport network resilience, 10.1680/jbren.21.00055.

Mitoulis, S.A., Argyroudis, S.A., Loli, M., Imam, B., 2021. Restoration models for quantifying flood resilience of bridges. Eng. Struct. 238, 112180.

Mitoulis, S.A., Argyroudis, S., Panteli, M., Fuggini, C., Valkaniotis, S., Hynes, W., Linkov, I., 2023. Conflict-resilience framework for critical infrastructure peacebuilding. Sustain. Cities Soc. 91, 104405.

Muslemani, H., Liang, X., Kaesehage, K., Ascui, F., Wilson, J., 2021. Opportunities and challenges for decarbonizing steel production by creating markets for 'green steel'products. J. Clean. Prod. 315, 128127.

Nahangi, M., Guven, G., Olanrewaju, B., Saxe, S., 2021. Embodied greenhouse gas assessment of a bridge: A comparison of preconstruction Building Information Model and construction records. J. Clean. Prod. 295, 126388 https://doi.org/10.1016/j.jclepro.2021.126388.

Noland, R.B., Hanson, C.S., 2015. Life-cycle greenhouse gas emissions associated with a highway reconstruction: A New Jersey case study. J. Clean. Prod. 107, 731–740. https://doi.org/10.1016/j.jclepro.2015.05.064.

Peng, J., Yang, Y., Bian, H., Zhang, J., Wang, L., 2022. Optimisation of maintenance strategy of deteriorating bridges considering sustainability criteria. Struct. Infrastruct. Eng. 18 (3), 395–411.

Piras, S., Palermo, A., Saiid Saiidi, M., 2022. State-of-the-Art of Posttensioned Rocking Bridge Substructure Systems. J. Bridg. Eng. 27 (3), 03122001.

Pizarro, A., Manfreda, S., Tubaldi, E., 2020. The science behind scour at bridge foundations: A review. Water 12 (2), 374.

Popescu, M.D., Drăgan, C., Borcea, D.R., Horvat, A., 2007. Quotation indicators for construction works, Vol 4. COCC, Bucharest.

Qian, J., Zheng, Y., Dong, Y., Wu, H., Guo, H., Zhang, J., 2022. Sustainability and resilience of steel–shape memory alloy reinforced concrete bridge under compound earthquakes and functional deterioration within entire life-cycle. Eng. Struct. 271, 114937.

Reza, B., Sadiq, R., Hewage, K., 2014. Emergy-based life cycle assessment (Em-LCA) for sustainability appraisal of infrastructure systems: a case study on paved roads. Clean Techn Environ Policy 16, 251–266. https://doi.org/10.1007/s10098-013-0615-5.

Sabău, M., Bompa, D.V., Silva, L.F., 2021. Comparative carbon emission assessments of recycled and natural aggregate concrete: Environmental influence of cement content. Geosci. Front. 12 (6), 101235 https://doi.org/10.1016/j.gsf.2021.101235.

Saha, D., 2018. Low-carbon infrastructure: an essential solution to climate change? Online. Available at: https://blogs.worldbank.org/ppps/low-carbon-infrastructure-essential-solution-climate-change, Accessed 27 Feb 2019.

San José, R., Pérez, J.L., Gonzalez-Barras, R.M., 2021. Assessment of mesoscale and microscale simulations of a NO2 episode supported by traffic modelling at microscopic level. Sci. Total Environ. 752, 141992 https://doi.org/10.1016/j.scitotenv.2020.141992.

Santero, N.J., Horvath, A., 2009. Global warming potential of pavements. Environ. Res. Lett. 4 (3), 034011.

Santos, J., Cerezo, V., Soudani, K., Bressi, S., 2018. A comparative life cycle assessment of hot mixes asphalt containing bituminous binder modified with waste and virgin polymers. Procedia cirp 69, 194–199.

Santos, J., Torres-Machi, C., Morillas, S., Cerezo, V., 2022. A fuzzy logic expert system for selecting optimal and sustainable life cycle maintenance and rehabilitation strategies for road pavements. Int. J. Pavement Eng. 23 (2), 425–437.

Saxe, S., Kasraian, D., 2020. Rethinking environmental LCA life stages for transport infrastructure to facilitate holistic assessment. J. Ind. Ecol. 24 (5), 1031–1046. https://doi.org/10.1111/jiec.13010.

Sayers, P. B., Horritt, M., Carr, S., Kay, A., Mauz, J., Lamb, R., Penning-Rowsell, E., 2020. Third UK Climate Change Risk Assessment (CCRA3): Future flood risk. Research undertaken by Sayers and Partners for the Committee on Climate Change. Published by Committee on Climate Change, London.

Shani, P., Chau, S., Swei, O., 2021. All roads lead to sustainability: Opportunities to reduce the life-cycle cost and global warming impact of US roadways. Resour. Conserv. Recycl. 173, 105701.

Sharif, S. A., Hammad, A., 2019. Simulation-based multi-objective optimization of institutional building renovation considering energy consumption, life-cycle cost and life-cycle assessment. J. Build. Eng. 21, 429-445.

Sharifi, F., Birt, A.G., Gu, C., Shelton, J., Farzaneh, R., Zietsman, J., Fraser, A., Chester, M., 2021. Regional CO2 impact assessment of road infrastructure improvements. Transport. Res. Part D: Transport Environ. 90, 102638. 10.1016/j.trd.2020.102638.

Smith, D.A., Spencer, P., Dolling, C., Hendy, C., 2015. Carbon calculator design tool for bridges. In Proceedings of the Institution of Civil Engineers-Bridge Engineering. 168(3), 232-244. 10.1680/jbren.13.00025.

Smith, A. W., Argyroudis, S. A., Winter, M. G., Mitoulis, S. A., 2021, December. Economic impact of bridge functionality loss from a resilience perspective: Queensferry Crossing, UK. In Proceedings of the Institution of Civil Engineers-Bridge Engineering, 174(4), 254-264.

Somboonpisan, J., Limsawasd, C., 2021. Environmental weight for bid evaluation to promote sustainability in highway construction projects. J. Constr. Eng. Manag. 147 (4), 04021013. https://doi.org/10.1061/(ASCE)CO.1943-7862.0002005.

Spain, B., 2014. Spon's Construction Resource Handbook. Spon Press.

Steele, K., Cole, G., Parke, G., Clarke, B., Harding, J., 2003. November. Highway bridges and environment—Sustainable perspectives. In Proceedings of the Institution of Civil Engineers-Civil Engineering, 156(4), 176-182. 10.1680/cien.2003.156.4.176 Thomas Telford Ltd.

Suhendro, B., 2014. Toward green concrete for better sustainable environment. Procedia Eng. 95, 305–320.

Tan, X., Mahjoubi, S., Zhang, Q., Dong, D., Bao, Y., 2022. Optimizing high-performance fiber-reinforced cementitious composites for improving bridge resilience and sustainability. J. Infrastruct. Preserv. Resilience 3 (1), 1–18.

The Concrete Centre, 2020. MPA Specifying Sustainable Concrete. The Concrete Centre, London, UK.

Thompson, P.D., Ford, K.M., 2012. Estimating life expectancies of highway assets: Guidebook, Vol. 1. Transportation Research Board.

Tsakalidis, A., Gkoumas, K., Pekár, F., 2020. Digital transformation supporting transport decarbonisation: technological developments in EU-funded research and innovation. Sustainability 12 (9), 3762.

Vishnu, N., Kameshwar, S., Padgett, J.E., 2022. Road transportation network hazard sustainability and resilience: correlations and comparisons. Struct. Infrastruct. Eng. 19 (3), 345–365.

Wan, C., Yang, Z., Zhang, D., Yan, X., Fan, S., 2018. Resilience in transportation systems: a systematic review and future directions. Transp. Rev. 38 (4), 479–498.

Wang, X., Duan, Z., Wu, L., Yang, D., 2015. Estimation of carbon dioxide emission in highway construction: A case study in southwest region of China. J. Clean. Prod. 103, 705–714.

Wang, Z., Yang, D.Y., Frangopol, D.M., Jin, W., 2020. Inclusion of environmental impacts in life-cycle cost analysis of bridge structures. Sustainable Resilient Infrastruct. 5 (4), 252–267.

Wardhana, K., Hadipriono, F.C., 2003. Analysis of recent bridge failures in the United States. J. Perform. Constr. Facil 17 (3), 144–150.

Zamanifar, M., Hartmann, T., 2021. Decision attributes for disaster recovery planning of transportation networks; A case study. Transp. Res. Part D: Transp. Environ. 93, 102771.

Zhang, N., Alipour, A., 2020. Two-stage model for optimized mitigation and recovery of bridge network with final goal of resilience. Transp. Res. Rec. 2674 (10), 114–123.